Recombination impacts damaging and disease mutations accumulation in human populations

Julie G. Hussin[1,2,3], Alan Hodgkinson[1,2], Youssef Idaghdour[1,2], Jean-Christophe Grenier[1], Jean-Philippe Goulet[2], Elias Gbeha[1], Elodie Hip-Ki[1], Philip Awadalla[1,2,*]

[1]Ste-Justine University Hospital Research Centre, Faculty of Medicine, University of Montreal, Canada;

[2]CARTaGENE Project, Ste-Justine University Hospital, Montreal, Canada;

[3] current address: Wellcome Trust Centre for Human Genetics, University of Oxford, UK;

*corresponding author: philip.awadalla@umontreal.ca

Many decades of theory have demonstrated that in non-recombining systems, slightly deleterious mutations accumulate non-reversibly[1], potentially driving the extinction of many asexual species. Non-recombining chromosomes in sexual organisms are thought to have degenerated in a similar fashion[2], however it is not clear the extent to which these processes operate along recombining chromosomes with highly variable rates of crossing over. Using high coverage sequencing data from over 1400 individuals, we show that recombination rate modulates the genomic distribution of putatively deleterious variants across the entire human genome. We find that exons in regions of low recombination are significantly enriched for deleterious and disease variants, a signature that varies in strength across worldwide human populations with different demographic histories. As low recombining regions are enriched for highly conserved genes with essential cellular functions and show an excess of mutations with demonstrated effect on health, this phenomenon likely affects disease susceptibility in humans.

The recent human demographic expansion has resulted in an excess of rare variants [3,4], a large proportion of which are putatively functional. Although these variants potentially have phenotypic effects, their distribution across the genome has yet to be fully characterized. Recombination (or linkage) is an important factor in determining the spatial distribution of these rare and potentially disease associated variants along the genome. In the absence of recombination, theory predicts that mildly disadvantageous mutations accumulate on haplotypes, as mutation-free haplotypes cannot be regenerated once they are lost - a process termed "Muller's

ratchet" [1,5]. Although mostly explored in asexual systems, evidence for this process has recently been described in non-recombining regions of model organisms such as in Drosophila [6,7] or, for mammalian Y-chromosomes, where the suppression of recombination is the primary model explaining why most Y-linked genes are no longer active [2], after an irreversible accumulation of genetic defects during millions of years.

Most of the human genome undergoes recombination, at a rate that varies dramatically between different genomic regions; large regions with low recombination called coldspots (CS) are punctuated by short hotspots of recombination where most of the crossovers occur, forming highly recombining regions (HRR) (Figure 1, online supporting note 1). In regions of the genome with low recombination rates, reduction of neutral genetic diversity is well-documented (Figure S1) [8,9]. Physical linkage of neutral variants to adaptive mutations, "selective sweeps", are likely to have a role in reducing this genetic variation [10,11], but background selection appears to be largely responsible for removal of neutral diversity linked to deleterious variants [11-13]. Functional variants may also have reduced frequency due to more complex processes, as these alleles can influence each other's evolutionary dynamics by competing with each other to become fixed within a population [14], a process known as Hill-Robertson interference [1,15]. Conversely, genetic recombination reduces interference by allowing these sites to segregate independently and generate new haplotypes, with the net effect of slowing down the accumulation of rare deleterious variants within exons [16].

The impact of recombination on diversity via Hill-Robertson interference is a long-standing question among evolutionary biologists, however the theoretical expectations have yet to be empirically demonstrated in human autosomes. Here, we ask whether variable recombination across the human genome has a significant impact on the spatial distribution of deleterious variation. Using single nucleotide variants (SNVs) from RNA and exome-sequencing data we generated for 521 French-Canadians (online supporting note 2) recruited by the CARTaGENE Project [17,18] and from high-coverage exome data in 911 individuals from non-admixed worldwide populations from the 1000 Genomes Project [19], we test whether putatively damaging variants accumulate differentially between CS and HRR. Annotation of all SNVs using public resources (Material and Methods) was done using five properties of mutations: the change in amino-acid sequences (non-synonymous or silent variants), the predicted impact on protein function and

structure (damaging variants), the level of conservation at the mutated coding site (constrained variants), the allele frequency (rare variants with minor allele frequency lower than 0.01) and the specificity of the variant within populations (private variants). For each category, we quantified the differential mutational burden between CS and HRR using odds ratios (ORs) to assess whether the fractions of mutations in the given category are significantly different between CS and HRR (Material and Methods).

For all populations, coldspots in the human genome show a higher proportion of rare and non-synonymous variants relative to regions of high recombination (Figure 2, Figure S2-S3). Rare and non-synonymous variants are enriched for mutations of functional importance, with potentially deleterious effects. As minor allele frequencies correlate positively with recombination rates (Table S2) [11], the site frequency spectrum differs between CS and HRR, with CS spectrum being skewed towards rarer alleles. In turn, common synonymous variants at unconstrained (neutral) sites are consistently enriched in HRR compared to CS in all populations. These findings suggest that purifying selection is more efficiently removing harmful variants in high recombining regions, whereas deleterious mutations survive in greater proportion when recombination frequencies are low. The results hold even after correcting for GC-content, average gene expression, substitution rates, types of mutations (transitions or transversions), exon size and total SNP density per exon (Table S2-S4, online supporting note 2). Importantly, the results are robust to a wide array of recombination rate thresholds used to define CS and HRR (Table S5). We also find that CS have larger introns than HRR (Figure S4, online supplementary note 4), consistent with the efficiency of selection being reduced in low recombining regions [6,20].

Next, we performed a series of analyses to test whether the genomic spatial distribution of deleterious variants is being modulated through variable Hill-Robertson interference effects in different recombination environments. First, we expect the extent of selective interference to be dependent on the number of negatively selected sites [14]. Therefore, we distributed exons into four uniform subgroups based on between-species conservation levels (Material and Methods, Figure S5), which allows for the comparison of exons with the same overall conservation, and thus similar functional importance, in CS and HRR. Conservation levels are determined using the conservation score GERP [21] that quantifies position-specific constraint based on the null hypothesis of neutral evolution. The enrichment of rare and putatively deleterious mutations is

seen in all conservation classes, showing that even when conservation is normalised across cold and hot regions, exons in coldspots are accumulating more damaging variants. Moreover, the effect is significantly reduced in classes of exons with lower conservation scores (Figure 3A, Figure S6). These exons likely have reduced numbers of negatively selected variants interacting with each other compared to more conserved exons with many sites under purifying selection. These observations strongly support that selective interference between deleterious variants underlies the observed enrichment of rare and non-synonymous variants in CS compared to HRR.

We then evaluated whether haplotypes within human exons have a higher mutational burden in CS compared to HRR using phased data from the 1000 Genomes Project. According to theory and simulations [1,22,23], deleterious variants will accumulate faster in low recombination regions in haploid systems, leading to an increased mutational load along individual haplotypes. We computed distributions of non-synonymous variants on haplotypes (Material and Methods), taking the exons as the basic unit, separating them into conservation categories such that compared exons exhibit similar levels of purifying selection. As expected, highly conserved exons tolerate a smaller number of non-synonymous mutations than exons with low conservation. Although within HRR a larger proportion of haplotypes carry at least one mutation compared to CS, because variants are more common and exons are larger (Figure S4), haplotypes with two and more non-synonymous mutations are found in significantly higher proportions in CS (Figure 3B, Figure S7). This effect is not seen for the least conserved exons, which are unlikely to be subject to high level of selective interference. Conversely, we observe a ~2-fold significant enrichment of the haplotype class with two non-synonymous variants in CS relative to HRR for the most conserved exons, where interference is likely stronger. Although phasing of rare variants remains technically challenging, phasing errors will tend to even out the rare variants across haplotypes, and is unlikely to drive the effect observed here. This differential haplotype burden is in line with a Muller's ratchet process where the least-loaded haplotype class, eroded by drift or mutation, is not replenished as fast when there is a lack of recombination, causing haplotypes with more than one deleterious variant to be slightly more frequent.

We also performed extensive computer simulations (online supporting note 3, Table S6) using forward-in-time simulators [24,25] to determine whether the above observations are consistent with interference between negatively selected mutations in diploid genomes with variable

recombination rates. Simulated coldspots show a higher proportion of rare and negatively selected mutations on haplotypes compared to HRR under a number of different demographic models (Table S7). These differences between recombination environments increase with the proportion of selected sites simulated and we find that a small proportion of strongly selected mutations is less impactful than many mutations with small effects. Models of background selection with no interference, harbouring only a single locus under strong negative selection, do not predict differences in the proportion of rare mutations between recombination environments (Figure S8). These simulation results strongly support that interference between mildly deleterious variants is required to generate the patterns of diversity we observed along human autosomes. However, fixed mutations under negative selection show no significant enrichment in simulated coldspots, indicating that selective interference within populations does not necessarily result in higher rates of fixation of deleterious mutations in diploid organisms [26], thereby causing inter-species divergence measures to be insensitive to these effects [27].

If selection is driving this process, we may expect to see variable effects in populations with different histories and effective population sizes. To compare effects across populations, we considered variants in highly covered exons across all datasets (Table S1). We found a relative enrichment for non-synonymous variants in CS compared to HRR in all populations (Figure 2A, Figure S2), but the effect is reduced in the African population compared to others. Furthermore, damaging variants are enriched in CS for French-Canadian, European and Asian populations but not for Africans, making this effect potentially modulated by demographic history. Examining population-specific variants in the five relatively recently diverged populations of European ancestry, these private variants are enriched in CS compared to HRR (Figure 2B), even after adjusting for GC-content and total SNP density (Table S2). Interestingly, this effect is also observed for variants that are private to the recently founded French-Canadian population. These mutations were either very rare in the source population, or they originated *de novo* since the founding of Quebec four hundreds years ago [28]. The potential reduction in the efficiency of purifying selection in coldspots is thus detectable over brief evolutionary time scales and suggests that selection may have been affecting the distribution of variants differentially along the genome in the recent past.

Finally, for each individual we computed the relative proportion of rare and non-synonymous variants in CS and HRR and the resulting odds ratios (ORs)(Figure 4). The distribution of per individual ORs reveals extensive differences between individuals and populations. Although at the population level, rare and non-synonymous variants are enriched in CS compared to HRR (Figure 2A), these effects are not observed at the individual level in Africans. For rare variants, Europeans and Asians all have significant ORs, but the mean individual OR is larger in Europeans. Strikingly, the FCQ population shows an increased variance relative to other populations and exhibits more extreme OR values. Furthermore, the shape of the distribution of the relative proportion of rare variants in CS differs slightly in FCQ (Figure 4B). For non-synonymous variants, few individuals among AFR, ASN and EUR exhibit significant ORs, whereas again, the FCQ distribution is remarkably different and shows a shift in mean towards larger and significant individual effects (Figure 4C and D). For private variants, French-Canadians is the most extreme of European populations, followed by Finns and Italians from Tuscany (Figure S9). To confirm these results, we sequenced the exomes of 96 of the FCQ individuals, which fully supported the differences seen in this population (Figure S10). These differences may be due to population sizes and demographic histories, as selection is overall less efficient in smaller populations [28], and could impact CS more strongly than HRR. The population-specific increase in the differential burden observed here may be due to complex recent demographic events and depart from Wright-Fisher's expectations (online supplementary note 3), such as serial founder effects or range expansions leading to higher variance in reproductive success, as observed in the French-Canadians genealogical data [29]. Therefore, complex demographic processes in humans may have impacted genetic variation and the effective strength of selection differentially along the genome through the history of the human peopling.

The irreversible accumulation of mildly deleterious mutations along haplotypes in low recombining regions can have damaging phenotypic effects in individuals carrying them, since genomic regions with high linkage disequilibrium show an excess of genes primordial for response to DNA repair and cell cycle progression [30]. Furthermore, CS are enriched for genes involved in protein metabolic processes, mRNA processing, organelle organisation and microtubule-based processes (Table S8). Selective interference between deleterious mutations may thus impact the genetic aetiology of human diseases. By examining sequence variants that

have a demonstrated effect on health reported in the ClinVar database [31], we found that for variants with MAF lower than 0.01 in humans, disease-related mutations reported in ClinVar are enriched in CS relative to HRR, with the effect driven mainly by the coldest regions in the human genome, with mean recombination rate lower than 0.1 cM/Mb (Figure 5). Conversely, a lack of common variants (MAF>0.1) implicated in human disease is notable in CS, possibly reflecting the higher power to find disease risk factors in highly tagged genomic regions in genome wide association studies. Moreover, ultra-sensitive regions of the genome, where a 400-fold enrichment of disease-causing mutations has previously been reported [32], are greatly enriched in CS (OR=6.506 [6.406; 6.607], Table S9). Finally, cancer genomes also exhibit a higher proportion of mutations within low recombining regions (Figure 5, Table S9), highlighting the importance of cold regions for genomic integrity and stability at the cellular level. Altogether, these results indicate that rare variants identified as medically relevant are more likely to be found in human coldspots, as new deleterious mutations occurring in regions with higher recombination rates will be more efficiently eliminated by natural selection.

Until now, selective interference had been empirically studied through inter-species divergence, and no effect of recombination on such measures had been detected in primates [27]. In contrast, these population genetic analyses reveal that the efficiency of selection depends on local recombination rates modulating selective interference, explaining the spectrum of rare functional variation. Consistent with evolutionary theory, the spatial distribution of deleterious mutations along the genome clearly varies according to recent population history and the unprecedented rapid expansion of human populations in recent times disproportionally affected essential genes occurring in regions of low recombination. The excess of rare disease mutations in these regions indicates that the reduction in selection efficiency likely impacts human health. Finally, given that genome-wide association studies have been powered by higher frequency variants, these results imply that a substantial proportion of undiscovered mutations associated with disease phenotype may be segregating in conserved low recombining regions.

Material and Methods

Genetic maps and recombination

We used three LD-based genetic maps [33], one pedigree map [34] and one admixture-based map [35] to identify 'cold' or 'hot' regions in the human genome that were shared across all human populations (Figure 1). The three LD-based maps were built from genotyping data from French-Canadians from Quebec (FCQ), CEU and YRI from HapMap3 (see Online Supporting Note 1). We used these maps to locate coldspots and hotspots of recombination. We define coldspots (CS) as regions of more than 50Kb with recombination rates between adjacent SNPs below 0.5 cM/Mb in FCQ, CEU and YRI populations. A hotspot is defined as a short segment (<15Kb) with recombination rates falling in the 90th percentile (> 5 cM/Mb). We define high recombination regions (HRR) as regions with a high density of hotspots, such that the distance separating neighbouring hotspots is smaller than 50 Kb. For each CS and HRR identified, we computed the mean recombination rate (cM/Mb) using deCODE pedigree-based map and the admixture-based African American map, and excluded all regions with inconsistent recombination rates in one of these maps. We obtained a list of 7,851 autosomal coldspots, spanning about a third of the human genome, for a total of 1.049 Gb (Table S1A). We identified 12,500 HRRs genome wide shared between FCQ, CEU and YRI populations, covering a total of 634.2 Mb. We verified that our results are robust to the choice in recombination parameters used to define regions (Table S5).

Genomic data

Genomic data from the 1000 Genome Project and the CARTaGENE project were used in this study. SNP calls for 911 individuals from 11 non-admixed populations from the 1000 Genomes Project Phase 1 high coverage exon-targeted data (50-100×) were downloaded from the 1000 genomes ftp site. Only SNPs called within targeted exons were extracted from vcf files. Details on 1000 Genomes populations, sequencing protocol, SNP calling, and validation can be found in the 1000 Genomes phase 1 publication [19]. Populations were then group by continent, with a total of 142,296 SNPs in 379 Europeans (EUR), 128,697 SNPs in 286 Asians (ASN) and 186,549 SNPs in 246 Africans (AFR) within 124,015 different exons. For the French-Canadian population, SNPs were called from RNA sequencing data (RNAseq), with a total of 178,394 SNPs in 521 individuals within expressed exons. RNAseq 100bp pair-ends indexed libraries were

constructed using the TruSeq RNASeq library kit (Illumina). Sequencing was done on HiSeq machines (Illumina), multiplexing three samples per lane. More details on the samples, the sequencing protocol and downstream analyses are described in supporting online note 2 and in [18]. Analyses comparing populations were done on a subset of exons that are highly covered (> 20×, HC exons) across all datasets. A total of 89,390 exons passed this filter, containing a total of 73,627 SNPs in FCQ, 69,672 in EUR, 63,726 in ASN and 89,789 in AFR (Table S1B). Additionally, all FCQ individuals were genotyped on the Illumina Omni2.5M array, and a subset of them (96 individuals) was exome sequenced on HiSeq machines (Illumina) with a total of 60,251 SNPs called (online supporting note 2).

Variant and exon annotations

We annotated SNPs either as synonymous or non-synonymous and those reported as intronic, in untranslated regions (UTR) or in non-coding RNA were labeled as 'other'. Functional annotations were obtained from three different sources (as of february 2013): Seattleseq (snp.gs.washington.edu/SeattleSeqAnnotation137), dbSNP (dbSNP135), and wAnnovar (wannovar.usc.edu) [36]. Functional annotations for non-synonymous mutations were obtained with PolyPhen2 and SIFT [37,38] and a variant was annotated as damaging when both methods predict the mutation to be damaging. Because there is a bias in these methods towards seeing a reference allele as benign, we excluded variants where the major allele was not the reference allele. Nonsense variants were annotated as damaging. We retrieved GERP conservation scores for all positions within the human exome (mendel.stanford.edu/SidowLab/downloads/ gerp/index.html) and PhyloP conservation scores from UCSC Genome website (hgdownload.cse.ucsc.edu/goldenpath/hg19/phyloP46way). We annotated a mutation as constrained if GERP > 3 and PhyloP > 1. Minor allele frequencies (MAF) were computed for each population independently and rare variants herein have a MAF < 0.01 within a population. SNPs with MAF > 0.01 are annotated as 'neutral' if they are synonymous and have both GERP < 3 and PhyloP < 1. For European populations, including FCQ, we annotated SNPs as private when they were unique to a population (not in other European populations nor in ASN and AFR) whereas shared variants are SNPs in common between all European populations. We also annotated exons by tabulating exon size, GC-content, average recombination rates in FCQ, CEU and YRI population genetic maps, average gene expression (computed from the FCQ RNAseq

data, online supplementary note 2), average GERP score, number of sites with GERP > 3, rate of synonymous substitutions per site (*dS*) between homologous gene sequences from human and chimp. *dS* values were retrieved from Ensembl as of November 2013, for 15,075 orthologous genes out of the 21,986 RefSeq genes and have been calculated by *codeml* in the PAML package [39]. Exons were ranked based on GC-content, GERP annotations, *dS* values and expression level, and stratified in four categories of equal sizes: low (25% lowest values), medium low (ranked between 25 and 50%), medium high (ranked between 50 and 75%) and high (25% highest values). For each exon and each population, we computed the number of SNPs, average MAF per population and the density (SNP/Kb) of non-synonymous, constrained and damaging variants.

Differential mutational burden

The mutational load reflects reduction in fitness for the population compared to a case where all individuals would have the most favored genotype at each site [40,41]. Odds Ratios (OR) are used to compare mutational loads between CS and HRR, based on the different types of mutations. We call this quantity differential mutational burden. The variant types analysed are *rare*, *non-synonymous*, *damaging*, *constrained*, *neutral*, *private*, *non-synonymous private* and *shared*. The OR for a variant type T is computed as:

$$OR_T = (N_{CS,T} \times X_{HRR,T}) / (N_{HRR,T} \times X_{CS,T})$$

with $N_{CS,T}$ and $N_{HRR,T}$ the number of variants annotated of type T and $X_{CS,T}$ and $X_{HRR,T}$ the number of other annotated variants in CS and HRR, respectively. Variants with missing annotations for a given type were excluded of the OR calculation for that type. Confidence intervals were calculated following the procedure described in [42]. Using alleles carried by each individual at all annotated variants, the differential mutational burden is also evaluated per individual. We consider zygosity per site, such that for a heterozygote at a non-synonymous site for example, both the non-synonymous allele and the reference allele are counted, and for a non-reference homozygote, the non-synonymous site is counted twice. We note that ignoring zygosity (counting each site once as either mutated or reference) does not change the distributions of individual ORs. Sites for which the reference allele is the derived allele (as inferred from chimp and rhesus macaque) were ignored in the per-individual OR calculation. We evaluated correlations between recombination rates and variant density in exons using linear regression

models, adjusting for expression level (online supporting note 2), GC-content, exon size and SNP density.

Haplotype load

Haplotypes from the 1000 Genomes populations were phased using ShapeIT2 using SNP array and sequence data (ftp://ftp.1000genomes.ebi.ac.uk/vol1/ftp/release/20110521/) as of November 2013 [43]. For each phased haplotype in an exon, we counted the number of non-synonymous mutations, and we computed haplotypes allelic classes [44], ie. the number of haplotypes with 0, 1, 2, …, n_{max} non-synonymous mutations. We identified 9 genes with exons that have an extremely high haplotype load: HRNR, FLG, MKI67, OR51B6, AHNAK2, PLIN4, CMYA5, MUC17, RP1L1. These genes were excluded from the analyses. After excluding these outlier exons, the maximum number n_{max} of non-synonymous mutations on a haplotype never exceeds 10. CS and HRR haplotype distribution were compared for exons in each conservation category. Conservation categories are based on a conservative ranking of exons according to both their average GERP scores and their number of sites with GERP > 3 (Figure S5). Confidence intervals for the proportions of haplotypes in each haplotype class are computed by resampling the same number of exons in CS and HRR in each conservation category.

Simulations

We perform forward simulations using SLiM and sfs_code [24,25]. For 250 diploid individuals, we simulated exon-like sequences with non-synonymous mutations, with $\theta = 0.001$ and N_e=1000, and tested models with the overall population recombination rate $\rho = \theta$ and $\rho = \theta/2$. We simulated human-like recombination environments, according to the average recombination rate and size of CS and HRR in the human exome: CS are 95 Kb long in average and contain 4.1% of recombination, HRR are 28 Kb long in average with 58.6% of recombination. Each simulated exome consists of 75 fragments of 200 Kb, with CS- and HRR-like sequences separated by 77Kb. Different demographic and selection models are studied (see online supporting note 3) with parameters inferred in previous studies [45,46]. The fitness effects for non-synonymous mutations are gamma distributed with mean *s,* with dominance coefficient $h = 0.5$ in all cases. We ignored positive selection in our models. We also performed simulations under null models, with constant ρ or without negative selection ($s = 0$), to evaluate expectations without variation in

recombination rates or under selective neutrality. For each simulation, mutations that have a derived allele frequency below 0.01 were annotated as *rare*. Non-synonymous mutations are site attributed a negative selection coefficient and were divided in 3 categories: non-synonymous with a selection coefficient larger than $-1/N_e$ (*ns*, effectively neutral), smaller than $-1/N_e$ (*nsneg*, negatively selected) and smaller than -0.01 (*nsdam*, damaging). The threshold for damaging variants is set to match the number of non-synonymous damaging variants in the empirical data. We used odds ratios to estimate the differential mutational load between CS and HRR for rare and non-synonymous mutations in simulations.

Disease mutations and genes

Clinical variants with potential and validated pathogenicity were retrieved from the curated ClinVar database [31] (https://www.ncbi.nlm.nih.gov/clinvar). Variants that are not segregating 1000 Genomes populations (which represent the vast majority of ClinVar variants), or that are found at a MAF lower than 0.01 in these populations, were classified as *rare*. ClinVar variants with MAF>0.1 were classified as *common*. ORs were computed by comparing these rare and common variants to non-disease variants with MAF in 1000 Genomes populations lower than 0.01 and larger than 0.1, respectively, between CS and HRR. These results were fully replicated using the Humsavar database (http://www.uniprot.org/docs/humsavar), which are disease mutations identified from the Universal Protein Resource (UniProt). Sensitive and ultra-sensitive regions coordinates were retrieved from [32], that have been examined for the presence of inherited disease-causing mutations from the Human Gene Mutation Database (HGMD). Somatic mutations from cancer genomes were retrieved from the COSMIC database (http://cancer.sanger.ac.uk/cancergenome/projects/cosmic). We used PANTHER [47] and WebGestalt [48] resources to perform gene set enrichment analyses. For WebGestalt, the reference list is the list of 21,987 genes included in the gtf file used to annotate exons (ftp://ftp.ensembl.org/pub/release-71/gtf/homo_sapiens/Homo_sapiens.GRCh37.71.gtf.gz).
PANTHER does not accept a reference list larger than 20,000 genes; the default Homo sapiens gene set was therefore used. The submitted gene list contains all annotate CS genes. Classification terms for “Biological Process” and “Molecular function” hierarchy were selected from the Gene Ontology (GO) vocabulary [49] if they were found significantly enriched with both

tools, with bonferroni correction applied in both. Highly significant GO terms found with WebGestalt but missing from PANTHER GO term list are also reported (Table S8).

Contributions and Acknowledgments: JH, AH, and PA designed the study. PA provided samples. EG and EHK processed samples for sequencing and genotyping. JCG and VB aligned sequencing data. JH, YI, AH, JCG, and JPG performed quality control on genotyping and sequencing data. JH performed the analyses. JH, AH, and PA wrote the manuscript. We thank Claude Bhérer, Greg Gibson, Gil McVean, John Novembre, Chris Spencer and Eric Stone for comments on the study, and the CARTaGENE participants and team for data collection. We acknowledge financial support from Fonds de la recherche en santé du Québec (FRSQ), Genome Quebec, Réseau de médecine génétique appliquée (RMGA), Fonds québécois de la recherche sur la nature et les technologies (FQRNT) and the Canadian Partnership Against Cancer. JH is a Human Frontiers Postdoctoral Fellow, AH is an FRSQ Research Fellow and YI is a Banting Postdoctoral Fellow. The authors declare no conflict of interests. Requests for CARTaGENE data published here should be submitted to the CARTaGENE program at philip.awadalla@cartagene.qc.ca or access@cartagene.qc.ca, citing this study. Other datasets are available from www.well.ox.ac.uk/~julieh/mshussin2014

Figures

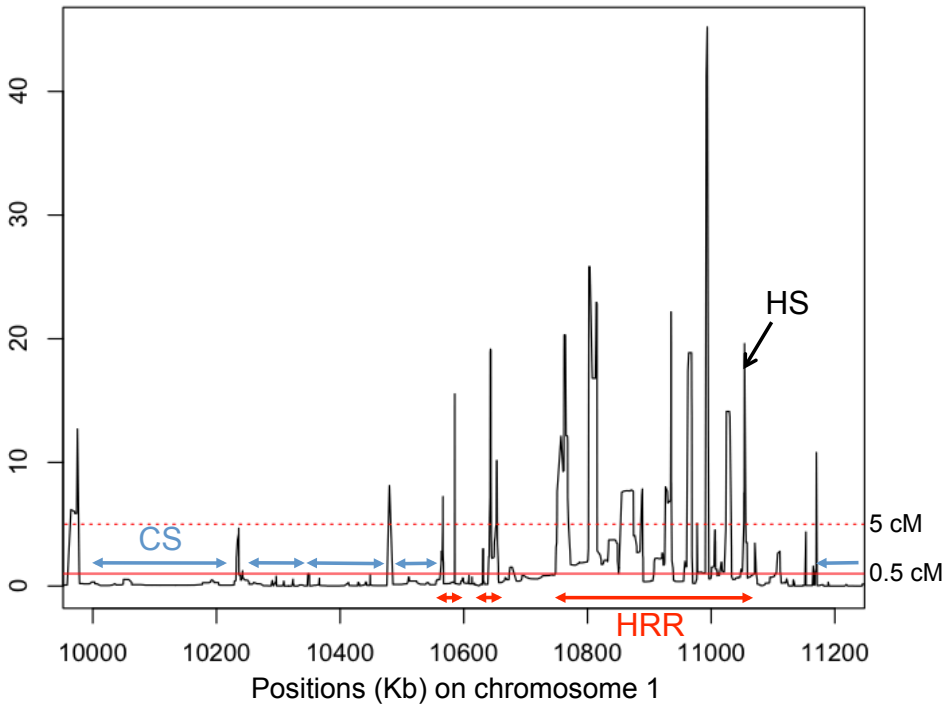

Figure 1. Coldspots (CS). Hotspots (HS) and High Recombination Regions (HRR).

CS are defined as regions of more than 50 Kb with recombination rates between adjacent SNPs below 0.5 cM/Mb. HS are defined as a short segment (<15Kb) with recombination rates above 5 cM/Mb. HRR are regions with a high density of hotspots, such that the distance separating neighbouring hotspots (>5 cM/Mb) is smaller than 50 Kb. CS and HRR have to be conserved across FCQ, CEU and YRI genetic maps and to have consistent recombination rates in admixture-based and pedigree genetic maps to be kept in our study (online supporting note 1).

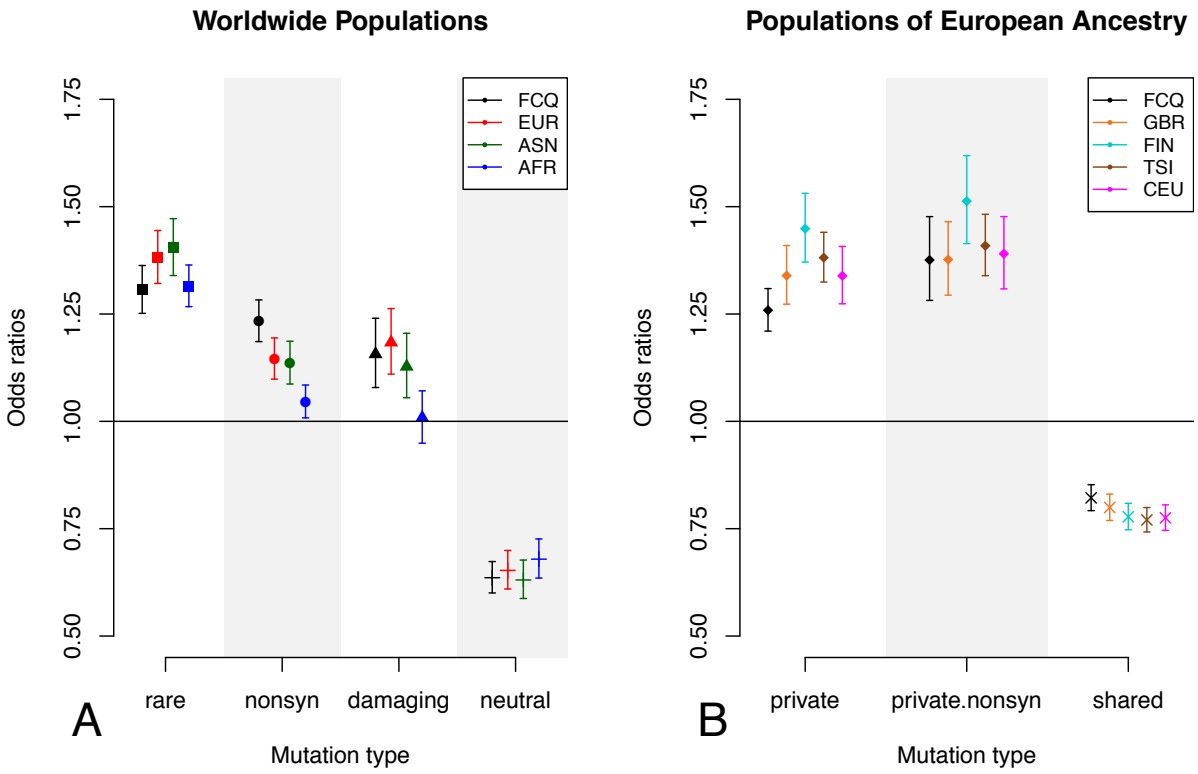

Figure 2. Differential mutational burden in Coldspots (CS) compared to Highly Recombining Regions (HRR) in human populations.

Differential burden is computed using odds ratios (OR), representing the relative enrichment of a category of variants compared to all variants in CS versus HRR (OR > 1 means enrichment in CS and OR < 1 means enrichment in HRR). Variants are categorized as rare (MAF<0.01 in a population), non-synonymous (missense and nonsense), damaging (predicted by both SIFT and Polyphen2), neutral (common and synonymous), private (specific to a population) and shared (present across populations). (A) Comparison of worldwide populations. ORs are computed based on variants called in exons from 521 French-Canadians of Quebec (FCQ), 379 Europeans (EUR), 286 Asians (ASN) and 246 Africans (AFR). (B) Comparison of closely related populations of West European ancestry. ORs are computed based on private and shared variants called in 96 French-Canadians of Quebec (FCQ), 89 British individuals (GBR), 93 Finns (FIN), 98 Italians from Tuscany (TSI) and 85 European Americans (CEU). Results for different subsets of genomic data are presented in Figure S2 and S3.

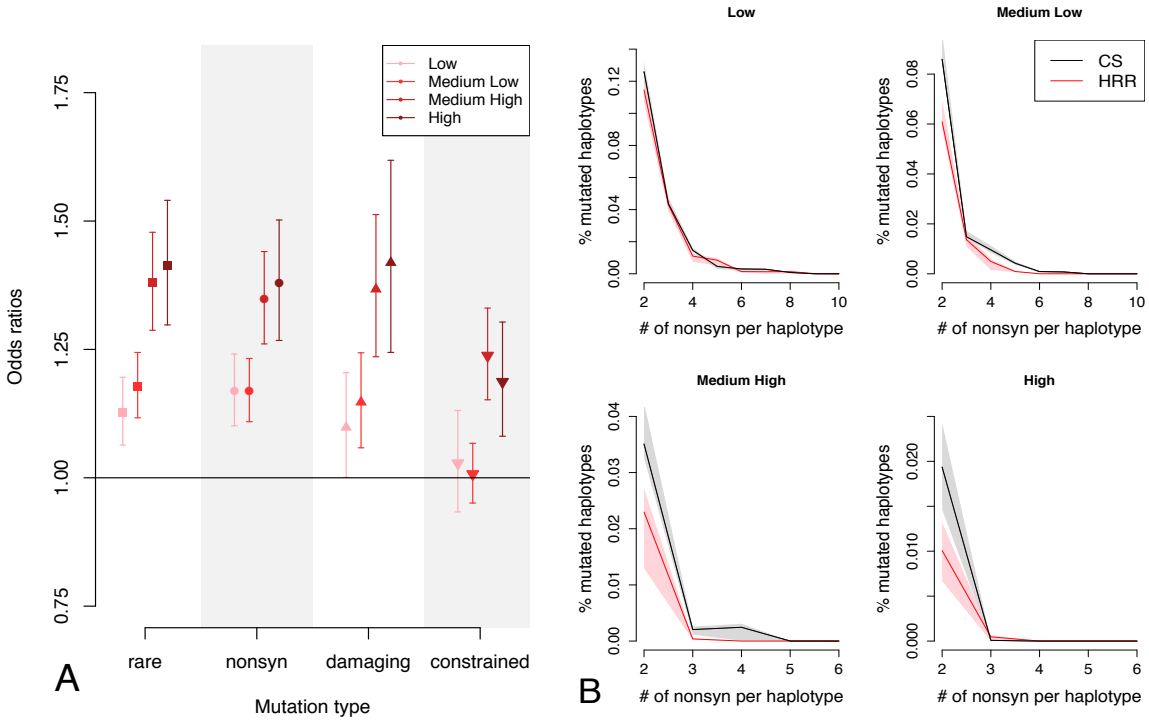

C Conservation Classes	Average GERP per bp	Number of constrained sites per bp (GERP>3)	Number of Exons			Number of SNPs (EUR)		
			Total	HRR	CS	Total	HRR	CS
Low	[-5.179; 1.103]	[0; 0.34]	47362	4554	13970	32166	9256	8323
Medium Low	[1.103; 2.613]	[0.34; 0.63]	39869	3215	13397	40115	10321	11910
Medium High	[2.613; 3.548]	[0.63; 0.75]	36089	2197	15191	24589	5250	9276
High	[3.548; 6.170]	[0.75; 1]	43416	1228	25602	17384	2661	9031

Figure 3: Differential mutational and haplotype burden as a function of conservation.

(A) Differential mutational burden between Coldspots (CS) and highly recombining regions (HRR) in Europeans (EUR) measured by Odds ratios for rare (MAF<0.01), non-synonymous (nonsyn), constrained (GERP < 3 and PhyloP < 1) and damaging variants, for exons binned in four conservation categories (Figure S5). (B) Haplotype load of non-synonymous variants in CS and HRR. For each conservation category, the proportion of mutated haplotypes with 2, 3, 4, etc. non-synonymous variants in Europeans (EUR) is plotted. The remaining proportion of mutated haplotypes with 1 variant (not plotted) is always larger in HRR than in CS. Confidence intervals are computed by resampling (Material and Methods). The proportion of mutated haplotypes in haplotype class 2 (haplotypes carrying two non-synonymous mutations) is significantly different between CS and HRR, except for the least conserved exons (C) Characteristics of exons in the four conservation categories in terms of average GERP score per base pair (bp) and number of constrained sites per bp (GERP>3). The number of exons and SNPs considered in plots presented in A and B are reported. Other populations show similar results (Figure S6, S7).

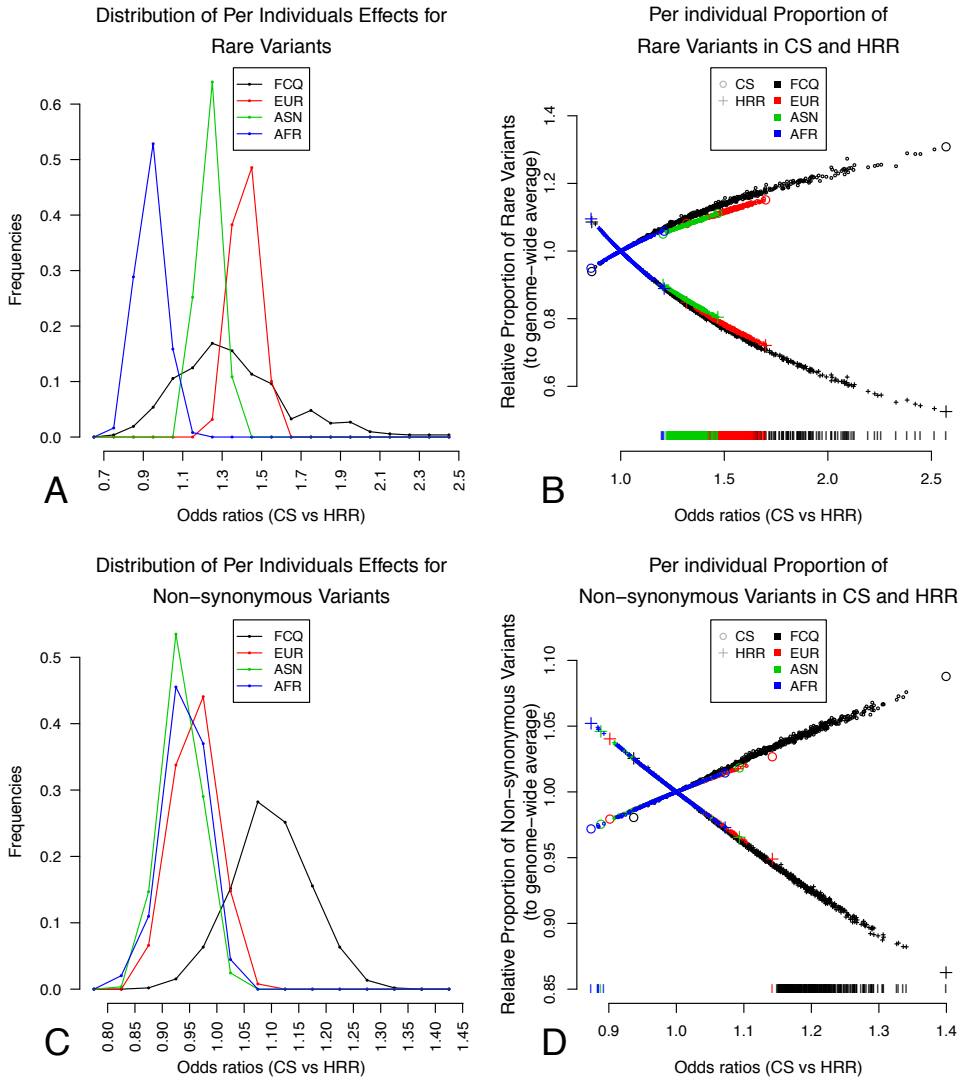

Figure 4. Per individual differential mutational burden across populations

Distribution of odds ratios (OR) per individual in French-Canadians, Europeans, Asians and Africans, comparing proportions of (A,B) rare and (C,D) non-synonymous mutations between coldspots (CS) and high recombining regions (HRR). The left panels (A,C) show the frequencies of individual OR in each population. Distributions are significantly different between populations for all comparisons (Kruskal-Wallis test, p<5e-9) except for AFR versus ASN non-synonymous OR distributions (Kruskal-Wallis test, p=0.051). The right panels (B,D) show, for each individual (ordered by their OR values), the relative proportions of rare or non-synonymous mutations in CS and HRR, computed by dividing CS and HRR proportions by genome-wide proportions of rare or non-synonymous variants within each individual, to adjust for differences across individuals. The larger symbols represent individuals with the minimum and maximum OR values in each population. Ticks at the bottom of the plots show individual OR values significantly different from 1 (two-tailed p<0.05). French-Canadian data used is the RNAseq dataset (online supporting note 2), replication with exome data of 96 French-Canadians is presented Figure S10.

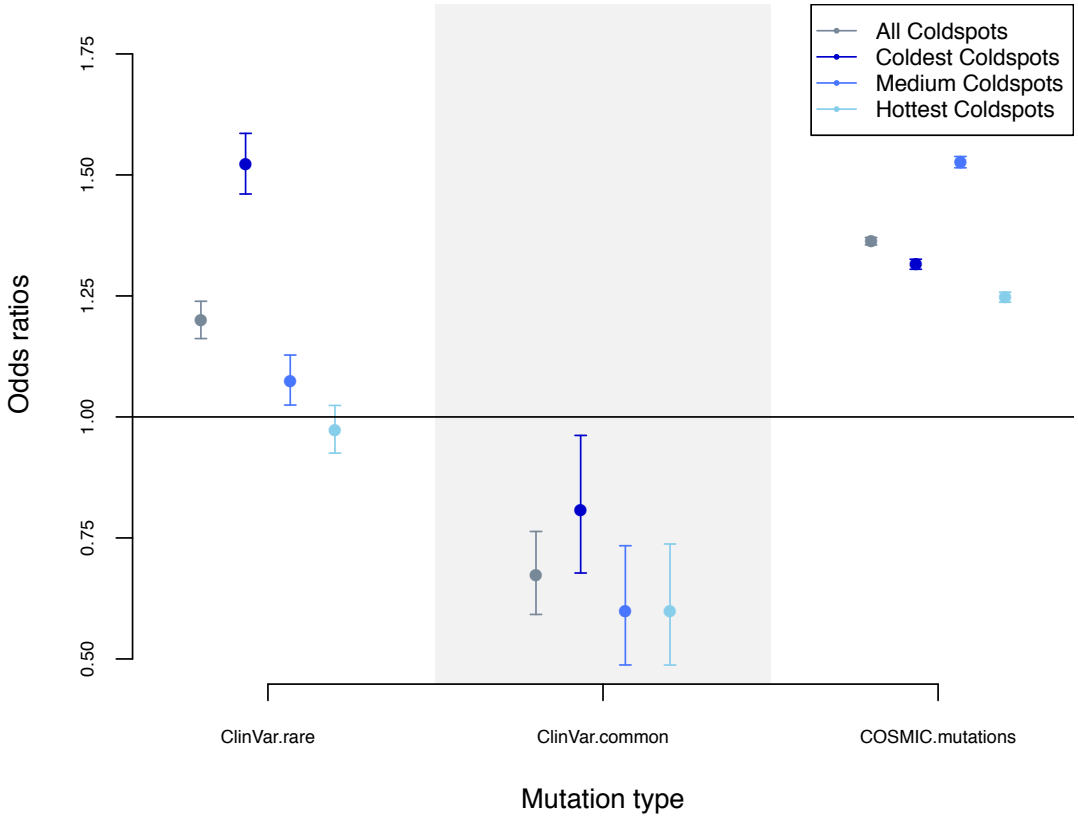

Figure 5. Differential mutational burden for disease and cancer mutations.

Differential burden is computed using odds ratios (OR), representing the relative enrichment of disease mutations from ClinVar database and cancer mutations from COSMIC database compared to variants in Coldspots versus High Recombining Regions found in 1000 Genomes populations at a given minor allele frequency (MAF). Rare ClinVar variants are either segregating at MAF below 0.01 or are not segregating in 1000 Genomes data overall. Common ClinVar variants have MAF > 0.1 in 1000 Genomes data overall. Coldspots are grouped into 3 categories: coldest (recombination rate r <0.1 cM/Mb), medium (0.1≤ r <0.15 cM/Mb) and hottest (0.15≤ r <0.5 cM/Mb) coldspots, such that each group roughly contains the same number of regions. Results correcting for sequence length instead of diversity for COSMIC mutations and ultra-sensitive regions are presented in Table S9.

References

1. Felsenstein, J. The evolutionary advantage of recombination. *Genetics* **78**, 737-56 (1974).

2. Charlesworth, B. & Charlesworth, D. The degeneration of Y chromosomes. *Philos Trans R Soc Lond B Biol Sci* **355**, 1563-72 (2000).

3. Keinan, A. & Clark, A.G. Recent explosive human population growth has resulted in an excess of rare genetic variants. *Science* **336**, 740-3 (2012).

4. Nelson, M.R. *et al.* An abundance of rare functional variants in 202 drug target genes sequenced in 14,002 people. *Science* **337**, 100-4 (2012).

5. Muller, H. The Relation of Recombination to Mutational Advance. *Mutat Res* **106**, 2-9 (1964).

6. Campos, J.L., Charlesworth, B. & Haddrill, P.R. Molecular evolution in nonrecombining regions of the Drosophila melanogaster genome. *Genome Biol Evol* **4**, 278-88 (2012).

7. Campos, J.L., Halligan, D.L., Haddrill, P.R. & Charlesworth, B. The Relation between Recombination Rate and Patterns of Molecular Evolution and Variation in Drosophila melanogaster. *Mol Biol Evol* **31**, 1010-28 (2014).

8. Hellmann, I. *et al.* Why do human diversity levels vary at a megabase scale? *Genome Res* **15**, 1222-31 (2005).

9. Lercher, M.J. & Hurst, L.D. Human SNP variability and mutation rate are higher in regions of high recombination. *Trends Genet* **18**, 337-40 (2002).

10. Hernandez, R.D. *et al.* Classic selective sweeps were rare in recent human evolution. *Science* **331**, 920-4 (2011).

11. Lohmueller, K.E. *et al.* Natural selection affects multiple aspects of genetic variation at putatively neutral sites across the human genome. *PLoS Genet* **7**, e1002326 (2011).

12. Charlesworth, B. The effects of deleterious mutations on evolution at linked sites. *Genetics* **190**, 5-22 (2012).

13. McGaugh, S.E. *et al.* Recombination modulates how selection affects linked sites in Drosophila. *PLoS Biol* **10**, e1001422 (2012).

14. Kaiser, V.B. & Charlesworth, B. The effects of deleterious mutations on evolution in non-recombining genomes. *Trends Genet* **25**, 9-12 (2009).

15. Hill, W.G. & Robertson, A. The effect of linkage on limits to artificial selection. *Genet Res* **8**, 269-94 (1966).

16. Keightley, P.D. & Otto, S.P. Interference among deleterious mutations favours sex and recombination in finite populations. *Nature* **443**, 89-92 (2006).

17. Awadalla, P. *et al.* Cohort profile of the CARTaGENE study: Quebec's population-based biobank for public health and personalized genomics. *Int J Epidemiol* (2012).

18. Hodgkinson, A. *et al.* High-resolution genomic analysis of human mitochondrial RNA sequence variation. *Science* **344**, 413-5 (2014).

19. Abecasis, G.R. *et al.* An integrated map of genetic variation from 1,092 human genomes. *Nature* **491**, 56-65 (2012).

20. Carvalho, A.B. & Clark, A.G. Intron size and natural selection. *Nature* **401**, 344 (1999).

21. Davydov, E.V. *et al.* Identifying a high fraction of the human genome to be under selective constraint using GERP++. *PLoS Comput Biol* **6**, e1001025 (2010).

22. Comeron, J.M., Williford, A. & Kliman, R.M. The Hill-Robertson effect: evolutionary consequences of weak selection and linkage in finite populations. *Heredity (Edinb)* **100**, 19-31 (2008).

23. Gordo, I., Navarro, A. & Charlesworth, B. Muller's ratchet and the pattern of variation at a neutral locus. *Genetics* **161**, 835-48 (2002).

24. Messer, P.W. SLiM: simulating evolution with selection and linkage. *Genetics* **194**, 1037-9 (2013).

25. Hernandez, R.D. A flexible forward simulator for populations subject to selection and demography. *Bioinformatics* **24**, 2786-7 (2008).

26. Charlesworth, B. & Charlesworth, D. Rapid fixation of deleterious alleles can be caused by Muller's ratchet. *Genet Res* **70**, 63-73 (1997).

27. Bullaughey, K., Przeworski, M. & Coop, G. No effect of recombination on the efficacy of natural selection in primates. *Genome Res* **18**, 544-54 (2008).

28. Casals, F. *et al.* Whole-exome sequencing reveals a rapid change in the frequency of rare functional variants in a founding population of humans. *PLoS Genet* **9**, e1003815 (2013).

29. Moreau, C. *et al.* Deep human genealogies reveal a selective advantage to be on an expanding wave front. *Science* **334**, 1148-50 (2011).

30. Smith, A.V., Thomas, D.J., Munro, H.M. & Abecasis, G.R. Sequence features in regions of weak and strong linkage disequilibrium. *Genome Res* **15**, 1519-34 (2005).

31. Landrum, M.J. *et al.* ClinVar: public archive of relationships among sequence variation and human phenotype. *Nucleic Acids Res* **42**, D980-5 (2014).

32. Khurana, E. *et al.* Integrative annotation of variants from 1092 humans: application to cancer genomics. *Science* **342**, 1235587 (2013).

33. HapMap Consortium *et al.* A second generation human haplotype map of over 3.1 million SNPs. *Nature* **449**, 851-61 (2007).

34. Kong, A. *et al.* Fine-scale recombination rate differences between sexes, populations and individuals. *Nature* **467**, 1099-103 (2010).

35. Hinch, A.G. *et al.* The landscape of recombination in African Americans. *Nature* **476**, 170-5 (2011).

36. Chang, X. & Wang, K. wANNOVAR: annotating genetic variants for personal genomes via the web. *J Med Genet* **49**, 433-6 (2012).

37. Adzhubei, I.A. *et al.* A method and server for predicting damaging missense mutations. *Nat Methods* **7**, 248-9 (2010).

38. Kumar, P., Henikoff, S. & Ng, P.C. Predicting the effects of coding non-synonymous variants on protein function using the SIFT algorithm. *Nat Protoc* **4**, 1073-81 (2009).

39. Yang, Z. PAML: a program package for phylogenetic analysis by maximum likelihood. *Comput Appl Biosci* **13**, 555-6 (1997).

40. Muller, H. Our load of mutations. *Am J Hum Genet* **2**, 111-76 (1950).

41. Agrawal, A.F. & Whitlock, M.C. Mutation load: the fitness of individuals in populations where deleterious alleles are abundant. *Annu. Rev. Ecol. Evol. Syst.*, 115–135 (2012).

42. Morris, J.A. & Gardner, M.J. Calculating confidence intervals for relative risks (odds ratios) and standardised ratios and rates. *Br Med J (Clin Res Ed)* **296**, 1313-6 (1988).

43. Delaneau, O., Zagury, J.F. & Marchini, J. Improved whole-chromosome phasing for disease and population genetic studies. *Nat Methods* **10**, 5-6 (2013).

44. Hussin, J., Nadeau, P., Lefebvre, J.F. & Labuda, D. Haplotype allelic classes for detecting ongoing positive selection. *BMC Bioinformatics* **11**, 65 (2010).

45. Eyre-Walker, A., Woolfit, M. & Phelps, T. The distribution of fitness effects of new deleterious amino acid mutations in humans. *Genetics* **173**, 891-900 (2006).

46. Boyko, A.R. *et al.* Assessing the evolutionary impact of amino acid mutations in the human genome. *PLoS Genet* **4**, e1000083 (2008).

47. Mi, H. *et al.* The PANTHER database of protein families, subfamilies, functions and pathways. *Nucleic Acids Res* **33**, D284-8 (2005).

48. Wang, J., Duncan, D., Shi, Z. & Zhang, B. WEB-based GEne SeT AnaLysis Toolkit (WebGestalt): update 2013. *Nucleic Acids Res* **41**, W77-83 (2013).

49. Ashburner, M. *et al.* Gene ontology: tool for the unification of biology. The Gene Ontology Consortium. *Nat Genet* **25**, 25-9 (2000).

Online Supporting Information

Online supporting note 1– Recombination analyses

1. Overview

Accurate population recombination maps are necessary to identify regions that are in different recombination environments. We used five population genetic maps (*1-3*), to identify 'cold' or 'hot' regions. We first identified these regions using LD-based population maps, and in a second step, we excluded regions for which recombination rates in pedigree and admixture maps were inconsistent with the definitions of the cold and hot regions.

2. Population genetic map of French-Canadians

We build the genetic map of the French-Canadians of Quebec (FCQ) population using LDhat (*4*). The 521 FCQ individuals were genotyped on the Illumina Omni2.5M array. A total of 1,554,440 autosomal SNPs were obtained after filtering (Quality control HWE $p<0.001$, Missingness < 0.05, MAF>0). We ran the *interval* program from the LDhat package on FCQ genotyping data. Because the likelihood tables for the *interval* program are pre-computed for a maximum number of 192 haplotypes, we randomly selected 96 unrelated individuals from the 521 FCQ individuals. The largest chromosomes (1 to 12) were broken into two segments (p and q arms) and all genomic segments were phased with ShapeIT2 (*5*). We ran the *interval* program on each genomic segment for 30,300,000 iterations with a burn-in of 300,000 iterations and sampled the population recombination rates ρ every 10,000 iterations. The estimate of the recombination rate ρ between each pair of adjacent SNPs, in units of $4N_e r$ per Kb, was computed by taking the average rate across iterations of the rjMCMC procedure implemented in *interval*. We sampled the population recombination rates ρ every 10,000 iterations. To convert the population recombination rate estimates in $4N_e r$ per Kb into centiMorgan per Megabase (cM/Mb), we inferred the effective population size N_e for the FC population using the estimates of r computed for the 2010 deCODE map in cM units (*2*). Specifically, we identified chromosomal segments

where both FCQ data and deCODE SNP positions allowed estimates of rates and we summed rates across these genomic regions to obtain the total estimated distance ($4N_eR$) and the total genetic distance (R in cM units) from the deCODE map.

3. Population genetic maps from HapMap3 data

Population genetic maps from the HapMap2 data have been built by the HapMap consortium in 2007 (*3*), using the 2002 deCODE pedigree map (*6*) and hg18 positions. It was subsequently 'lifted over' to hg19 using the UCSC liftOver tool and regions where the order of markers had changed were removed from the final maps. We re-computed the HapMap maps for CEU and YRI with the methodology used to compute the FCQ map described above to allow direct comparison. Specifically, we performed a lift over on the HapMap3 SNPs positions prior to estimating recombination rates with *interval* using 96 unrelated individuals from the CEU and YRI populations. We then converted the recombination rates in cM/Mb using the 2010 deCODE pedigree map (*2*), and obtained new HapMap genetic maps for these populations. These maps are available here: www.well.ox.ac.uk/~julieh/mshussin2014

4. Coldspots and High Recombining Regions

We used these genetic maps to locate coldspots and hotspots of recombination. We define coldspots (CS) as regions of more than 50Kb with recombination rates between adjacent SNPs below 0.5 cM/Mb in FCQ, CEU and YRI populations, such that they are shared between all human populations studied. We excluded centromeric regions and required that at least 5 SNPs support the coldspot, to avoid regions with dramatically reduced diversity, where power to estimate recombination rates is decreased. For each region identified, we computed the mean recombination rate (cM/Mb) using the deCODE pedigree map (*2*) and the admixture-based African American map (*1*), and we excluded all regions that have a recombination rate larger than 0.5 cM/Mb in one of these maps. We obtained a list of 7,851 autosomal CS, spanning about a third of the human genome, for a total of 1.049 Gb (Table S1). A hotspot is defined as a short segment (<15Kb) with recombination rates falling in the 90th percentile (> 5 cM/Mb). We define high recombination regions (HRR) as regions with a high density of hotspots, such that the

distance separating neighbouring hotspots is smaller than 50 Kb. We identified 12,500 HRRs genome wide shared between FC, CEU and YRI populations, covering a total of 634.2 Mb (Table S1). The definition of coldspot, hotspot and HRR are illustrated in Figure 1. A complete list of these regions can be found at www.well.ox.ac.uk/~julieh/mshussin2014. The recombination rate thresholds used to define coldspots and hotspot were chosen to maximize the overall number of SNPs included in the analyses while minimizing the difference between the number of SNPs in coldpots and in HRRs. The effects are robust to different recombination thresholds (Table S5).

Online Supporting Note 2 – French-Canadian Genomic Data

1. Overview

The main analyses for the French-Canadian (FCQ) population rely on SNPs called from RNA sequencing (RNAseq) data. SNPs from other populations come from the 1000 Genomes phase I high coverage exome dataset. We performed extensive analyses to ensure that calling SNPs from transcriptomes do not create biases influencing our population genetic analyses and cannot explain the difference seen in the FCQ population. We also performed exome sequencing for a subset of FCQ individuals for which we had RNAseq data and further validated SNP calls and the overall results found with the RNAseq SNPs.

2. French Canadians

The CARTaGENE project (CaG) collected biologicals and data from 20,000 participants recruited throughout the province of Quebec (*7*), and high-density genotyping and RNA sequencing data was generated for 521 French-Canadians participants (Material and Methods). Sampling includes individuals from three distinct metropolitan regions of Quebec: the Montreal area (MTL), Quebec City (QCC) and the Saguenay Lac-St-Jean region (SAG) (Figure S11). Regional origins of the individuals were validated with a principal component analysis (PCA) of genetic diversity using genotypic data and including individuals from the Reference Panel of Quebec (RPQ) (*8*). Population structure is complex and made of regionally differentiated populations (Figure S11), resulting from the very recent regional founder effect that occurred in Saguenay. This territory was colonized during the 19th century by a reduced number of settlers, who contributed massively to the genetic pool of individuals living in this region today (*9*).

3. Processing of the raw RNAseq Data and SNP calling

Approximately 3 mL of blood was collected for RNA work in Tempus Blood RNA Tubes (Life Technologies). Total RNA was extracted using a Tempus Spin RNA Isolation kit followed by

globin mRNA depletion by using a GLOBINclear-Human kit (Life Technologies). RNAseq 100bp pair-ends indexed libraries were constructed using the TruSeq RNASeq library kit (Illumina). Sequencing was done on HiSeq machines (Illumina), multiplexing three samples per lane. After initial filtering based on sequencing read quality, paired-end reads were aligned using TopHat (V1.4.0) (*10*) to the hg19 European Major Allele Reference Genome (*11*). PCR removal was performed using Picard (picard_tools/1.56, http://picard.sourceforge.net). Raw gene-level counts data were generated using htseq 0.5.3p3 (*12*). These counts were then normalized using EDASeq v1.4.0 and a procedure that adjust for GC-content as well as for distributional differences between and within sequencing lanes (*13, 14*). Average normalized gene expression levels per gene were determined by averaging expression levels of each gene across all individuals (Idaghdour et al. 2014. *In preparation*). Every exon of a gene was attributed the gene-level value.

SNP were called from RNAseq data using a procedure similar to SNP calling in exome sequencing data. However, prior to SNP calling, bowtie2 (0.12.7)(*15*) was used to removed abundant sequences (polyA, polyT, tRNA). Only reads that were properly paired and uniquely mapped were kept. Mapping quality score were recalibrated using GATK (*16*) and SNP calling was performed with samtools (0.1.18) (*17*). Filtering of SNPs was done using vcftools v0.1.7 (*18*). We kept SNPs with variant quality of 30 and genotype quality of 20 (Phred scores). Minor allele frequencies (MAF), the proportion of individuals with non-missing genotypes and Hardy-Weinberg equilibrium (HWE) p-values were computed using plink v1.07. SNPs showing departures from HWE at $p < 0.001$ were excluded. We obtained a total of 178,394 polymorphic SNPs (MAF > 0) in the 521 French-Canadians individuals (Table S1B).

4. Selection of Highly Covered Exons

To insure that sequencing SNPs are called throughout the length of exons and to reduce the possible biases due to read depth, we selected highly covered exons (hereafter termed HC exons) with all positions of their sequence covered at a minimum of 20× in more than 50% of the sequenced individuals (i.e. at least 261 FCQ individuals). We used BAMStats-1.25 to obtain the minimum coverage per exon per individual for 208,226 autosomal exons. A total of 89,390 exons

passed this stringent filter containing a total of 73,627 SNPs. For subsequent analyses, we also excluded 9 genes for which the mutational profiles were abnormal (Material and Methods).

5. FCQ Exome Sequencing Data and Genotyping

All individuals were also genotyped on the Illumina Omni2.5M array. A total of 1,554,440 autosomal SNPs were obtained after filtering (Quality control HWE $p<0.001$, MAF>0). We took all positions in common between the Omni2.5 chip and the RNAseq SNPs called. We filtered for missingness (<50% for RNAseq, <95% Omni) and filtered out positions for which the alleles did not match between the chip and RNAseq after flipping, ending up with 26,615 positions to compare. We compared genotypes for which there was a call in both datasets, and the concordance rates were above 98.8% in all individuals, with mean across individuals of 99.3%.

Exome sequencing was also performed for 96 FCQ individuals. DNA from each sample was extracted from peripheral blood cells and paired-end exome sequencing was performed on HiSeq machines (Illumina), multiplexing six samples per lane. We first performed trimming of sequencing read data using Trim Galore prior alignment to trim adaptors (with parameter –q 0, www.bioinformatics.babraham.ac.uk/projects/trim_galore). Alignment was performed using BWA version 0.5.9-r16. After recalibration with GATK (*16*), reads were trimmed for quality using bamUtil version 1.0.2 (genome.sph.umich.edu/wiki/BamUtil). SNP calling was performed with samtools (0.1.18) (*17*) using only properly paired and uniquely mapped reads. We kept SNPs with variant quality of 30 and genotype quality of 20 and minimum coverage of 10×, for a total of 60,251 SNPs. Using the concordance procedure described above, we computed concordance rates between the exome dataset and the RNAseq dataset for 30,850 SNPs called in both datasets. The mean concordance rate across individuals is 99.01%. There is one outlier individual with concordance rate of 94.8% (although its concordance rate between RNAseq and genotyping is 99.27%), all other individuals have concordance rate above 98%.

6. Checks in the FCQ dataset

Many additional analyses were performed on the FCQ data to insure the robustness of the results:

- We evaluated differences in diversity between CS and HRR in FCQ (Figure S1), replicating the documented observation of decreased diversity in CS.
- To ensure that the differences in the effects observed in FCQ are not due to biases in the RNAseq data, all results were derived with both RNAseq SNPs, and re-sequencing data of exomes in 96 individuals (Figure S2A, Figure S10). To evaluate the effect of private variants (Figure 2B, Figure S9), we used the exome sequencing dataset of 96 individuals.
- We evaluated the effect of confounding factors (Table S2-S5). The results are robust to GC content, expression levels and between-species neutral substitution rates (Table S3). Furthermore, we regressed the number of mutations of different types per exon on the recombination rate per exon, controlling for GC content, expression levels, exon size and total SNP density (Table S2). The effect is seen for all mutation types, with no marked differences between transitions and transversions or for mutations towards GC (Table S4), excluding the possibility that GC-biased gene conversion is responsible for the differences seen between recombination environments. Finally, we tested the effect using a wide array of recombination rate thresholds used to define CS and HRRs (Table S5).
- We computed OR for non-synonymous and damaging mutations for different frequency classes, to verify that the enrichment of potentially deleterious mutation is not only due to an enrichment of rare variants, that include more non-synonymous variants (Figure S3).

Similar checks were performed in the 1000 Genomes populations. In particular, we performed analyses using the highly covered exons from the RNAseq datasets as well as using all exons where SNPs were called in the 1000 Genomes populations (Figure S2). For other checks (confounding factors, frequency classes) the results obtained are generally the same as in the FCQ, therefore only the FCQ results are shown.

Online Supporting Note 3 – Simulations

1. Overview

In the past, selective interference leading to Muller's ratchet has been mainly investigated through simulation studies. These studies demonstrated the impact of no recombination on the accumulation of deleterious mutations within genomes (*19-23*). However, most results were produced for haploid genomes (but see (*24*)) and were set up to compared regions of free recombination with regions that entirely lack recombination. Here, we performed additional computer simulations (with SLiM (*25*) and sfs_code (*26*)) to describe the expectations under a model of selective interference between negatively selected mutations in diploid genomes, with recombination environments comparable to the ones observed in human autosomes. Both forward-in-time simulation programs gave similar results for all analyses.

2. Recombination environments

We simulated diploid genomes with a distribution of recombination rates similar to the one observed in the empirical data. For 250 individuals, we simulated exon-like sequences with non-synonymous mutations, with $\theta = 0.001$ and $N_e = 1000$, chosen to minimize computing time while getting diversity data comparable to human data. We tested models with the overall population recombination rate being $\rho = \theta$ or $\rho = \theta/2$, to evaluate whether the relationship between ρ and θ had an impact. We defined three recombination environments: coldspots (CS), high recombining regions (HRR) and regions in between. In the human exome, CS and HRR contain 4.1% and 58.6% of recombination events, respectively. These values were used in the simulations to match the human genetic map. For each genome, we simulated 75 fragments of 200Kb, with CS and HRR of 95 Kb and 28 Kb, respectively, and 77Kb of regions in between HRR and CS. We also simulated a null model with constant ρ, to insure that the effects seen do not reflect the difference in region length between CS and HRR.

3. Selection and demography

Our simplest model is a constant population size model with the distribution of fitness effects estimated by Eyre-Walker and colleagues (*27*), using their model without correction for demography (EW model). We also used other scenarios to model European and African human data, with parameters taken from the EA and AA models from (*28*), a study that inferred both selection and demographic parameters simultaneously. Finally, we simulate data under a model without selection (NTR), a control under selective neutrality but with the human-specific recombination map. The description of these models is shown in Table S6. For each model, we generated 100 replicates. Each replicate took between 15 and 55 hours to run, depending on the model and on the simulation program.

4. Differential Mutational and Haplotypes Load in Simulations

Odds ratios are used to estimate the differential mutational load between CS and HRR for rare and non-synonymous mutations (Material and Methods). Mutations with derived allele frequency (DAF) below 0.01 are labelled as *rare*. A proportion p of non-synonymous variants are attributed a selection coefficient from a gamma distribution of mean s. We make p take value from 0.1 to 0.75 and s takes values from -0.0294 to -0.3. Mutations with s larger than $-1/2N_e$ (*ns*) are effectively neutral, and others are negatively selected (*nsneg*). To model damaging mutations, we chose the threshold of below s = -0.01 (*nsdam*), to match the number of non-synonymous damaging variants in the empirical data.

Simulated CS have a higher proportion of *rare* and *nsneg* mutations than simulated HRR for all models of selective interference with $\rho = \theta$. Results for $\rho = \theta/2$ are highly similar, although the effect is somewhat reduced (Table S7A). The neutral model with varying recombination rates does not show an enrichment of rare variants in CS, indicating that the reduction of N_e in low recombination region alone does not account for the excess of rare variants. We find that the effect increases with p (Figure S8). We simulated a scenario with $p = 0.1$ and s = -0.3, such that the overall selective pressure acting on the loci is approximately the same as for $p = 0.75$ and s = -0.0425 (*27*). Interestingly, this model did not performed better than the scenario with $p = 0.1$ and

s = -0.0425, suggesting that small proportion of strongly selected mutations is unlikely to cause the difference in mutational load observed in the data. Scenarios modelling background selection with no interference further confirm this result: we simulated a single motif of 10bp in the centre of each region, where all sites have fixed s = 0.05, 0.1 or 0.15. These scenarios do not predict differences in the proportion of rare mutations between CS and HRR, indicating that background selection acting at one locus only does not lead to an enrichment of rare variants in regions with reduced N_e. Therefore, these results show that many mutations with small effects are required to reduce the efficiency of selection in CS.

We estimated the haplotype load by evaluating the proportion of variants of a given type per haplotype. We counted the number of replicates where the haplotype load is smaller in CS than HRR, to obtain a one-tailed *p*-value (Table S7B). Models with interference are predicted to result in a higher mutational load in CS for *rare*, *nsneg* and *nsdam* mutations after correcting for SNP density. However, background selection without interference does not lead to differential haplotype load between recombination environments. We also tested the expectation of the haplotype load under neutrality, to ensure that the differential linkage between CS and HRR is not biasing the expected distribution of haplotypes. These results strongly suggest that the effect observed in the genomic human data is caused by reduced selection efficiency due to interference between mildly deleterious variants.

5. Simulation of various demographic scenarios

In analyses of the genomic data, differences in the empirical distribution of odds ratios (OR) per individual are observed (Figure 4, Figure S9). They may be related to changes in N_e, such that smaller populations are even less efficiently purging variants from coldspots than large populations. However, none of the simulated scenarios described above showed significant differences in the distributions of individual OR computed for rare variants. In particular, no significant shift in the OR distribution for rare variants was seen between EA and AA scenarios (Table S6). We also simulated scenarios with population splits, with and without migration between populations and with the dominance coefficient h = 0.1. These models also failed to show significant differences between individual OR distributions. To try to understand the

observed differences between FCQ and other populations for distributions of individual OR for rare and non-synonymous variants (Figure 4, S9 and S10), several more complex demographic scenarios, with severe bottlenecks and/or with rapid expansions were tested with both SLiM and sfs_code, but none recapitulated the significant difference between distributions seen between the FCQ population and the others (Figure 4).

One possible explanation for this result is that simulation tools fail to adequately model recent population demography of human populations. Although changes in population size can be modelled with these tools, modelling spatial expansion may be essential to get more realistic simulation results. Unfortunately, although spatially explicit simulation tools allowing for complex demography and variation in recombination have been developed (*29*), selection models are not yet included. Furthermore, most simulation tools assume Poisson variance in reproductive success, an assumption often violated in populations with high fertility rates, as it was the case during French-Canadian expansion (*30, 31*). When only few parents contribute to the next generation (*32*), the larger than Poisson variance in family sizes introduces additional stochasticity, causing strong intergenerational genetic drift. Therefore, extensions of simulation methods in the future, to include these additional demographic parameters in flexible simulation frameworks with recombination and selection, will hopefully be informative to understand the impact of complex demography on selective interference. In any case, these results suggest that complex demographic processes, not generally accounted for in population genetics models of human peopling (*33*), may need to be considered to understand the differences in the genomic distribution of deleterious genetic variation.

Online Supporting Note 4 – Additional Analyses

1. SNP Functional Annotations

The functional impact of non-synonymous mutations was obtained with widely used prediction tools: PolyPhen (*34*) and SIFT(*35*), which both have high sensitivity but low specificity (*36*). We thus used a combination of the two methods to reduce the number of false positives. To estimate the level of constraint at nucleotides, we retrieved GERP conservation scores for all positions within the human exome. GERP scores were obtained from the Sidow lab website (http://mendel.stanford.edu/SidowLab/downloads/gerp/index.html). To reduce false positives, we further obtained PhyloP scores from UCSC Genome Bioinformatics website (http://hgdownload.cse.ucsc.edu/goldenpath/hg19/phyloP46way/). We annotated a mutation as constrained if GERP > 3 and PhyloP > 1. Sites with PhyloP > 1 are the top 10% of conserved sites in the human genome. The GERP threshold was chosen to be comparable to the PhyloP threshold, such that the overall proportion of SNPs and missense SNPs inferred as constrained is the same for both methods. We compared GERP and PhyloP conservations scores with Polyphen and SIFT predictions in the FCQ dataset. Overall, more than half non-synonymous mutations and a large proportion of damaging mutations (78.2%) are conserved according to both conservation scores, although GERP predictions concord slightly better with functional annotations than PhyloP predictions. We thus decided to use GERP predictions to classify exons in conservation categories.

2. Recombination and expression

Expression level of a gene is one of the best predictors of its evolutionary rate (*37*) with the efficiency of selection being weaker in lowly expressed genes. Therefore, we controlled for expression levels in our analyses (Table S2 and S3) and showed that our results are robust to variation in expression levels. However, we note that when analysing highly covered exons, the analyses are biased towards constitutively highly expressed genes. Interestingly, the effects are generally larger for this set of exons relative to all exons in the 1000 Genomes dataset (Figure S2), suggesting that relationship between mutational load, recombination and expression may be

of importance. Furthermore, it has been reported that within-gene recombination rates appear to correlate with transcription patterns, such as expression breadth and allelic expression (*38*). We observed a weak but significant negative correlation between recombination rates and mean gene expression in the FCQ data (Table S2), providing further support for a negative association between recombination and transcription in humans.

3. Introns and exon sizes

We computed the distribution of exon and intron lengths in high recombining regions (HRR) and in coldspots (CS) (Figure S4). Exons are larger in HRR than in CS and the length distribution are significantly different (Kruskal-Wallis chi-squared = 2089.667, df = 1, p-value < 2. $\times 10^{-16}$). The mean length of exons in HRR and CS are 534 bp and 284 bp, respectively. Conversely, introns are larger in CS than in HRR (Kruskal-Wallis chi-squared = 57.495, p = 3.388×10^{-14}). Excluding introns longer than 10Kb, the mean length of introns in CS and HRR are 2.313 Kb and 2.260 Kb, respectively ($p=8.303 \times 10^{-12}$). This confirms the overall negative relationship between intron length and recombination in humans, previously observed on a small set of introns using large-scale recombination rates (*39*). It has been suggested that strong selection favours deletion bias and intron contraction in humans and Drosophila (*40-43*), therefore these results are consistent with the efficiency of selection being reduced in human CS, leading to larger intron sizes in these genomic regions.

4. Pseudogenes, Gene Ontology and Disease Genes

We retrieved coordinates of the 17,216 regions annotated as pseudogenes from UCSC Tables (http://genome.ucsc.edu/cgi-bin/hgTables), covering 26,222 Kb of sequence. In total, 36% of these regions are in CS and 14% are in HRR. Pseudogenes overlap 9,411 Kb (0.89%) of CS and 3,610Kb of HRR (0.57%). These differences are significant (OR = 1.58 [1.52;1.64]). This result raises the possibility that more genes have lost their protein-coding ability in low recombining regions of the human genome, although an alternative explanation is that more gene duplication

were retained within CS throughout evolution, making gene function redundant and not required for survival.

To further characterize the potential impact on phenotypes, we performed a gene set enrichment analysis, using human gene annotations from the Gene Ontology database (*44*). CS are enriched for genes involved in essential biological processes such as cell cycle, mitosis, protein metabolic processes, mRNA processing, organelle organisation and microtubule-based processes. Most proteins coded by CS genes are binding proteins (nucleotide, RNA and ATP binding), ligase or transferase (Table S8).

Supplementary Figures

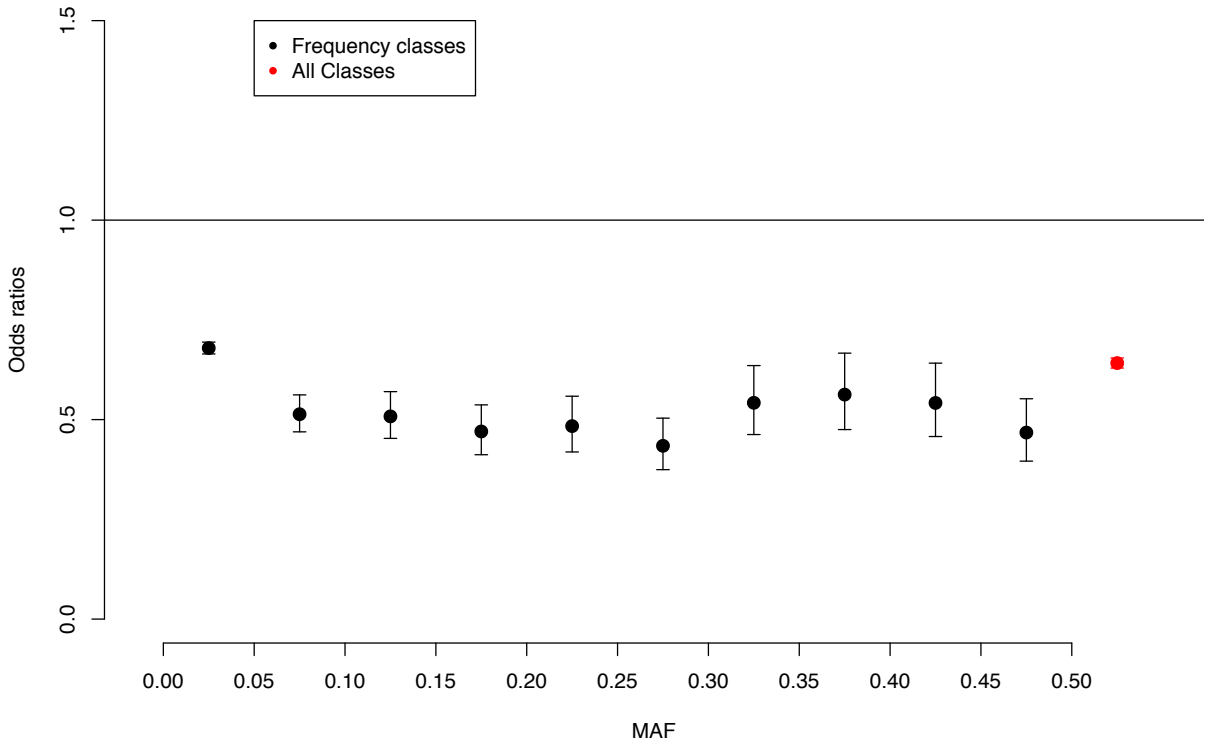

Figure S1. Comparison of levels of diversity between Coldspots (CS) and High Recombining Regions (HRR) for SNPs in the FCQ dataset.

Odds ratios (OR) are computed to compare SNP density between CS and HRRs for all SNPs (red) and SNPs divided in different allele frequencies classes (black). OR < 1 means that diversity is greater in HRR than in CS. We confirm the lack of diversity in CS relative to HRR, in line with previous evidence that diversity is reduced in low recombining regions. The effect is seen for all frequency classes and does not differ significantly between classes of SNPs with MAF > 0.05. The class of variants with MAF < 0.05 shows a slightly smaller effect than the other frequency classes.

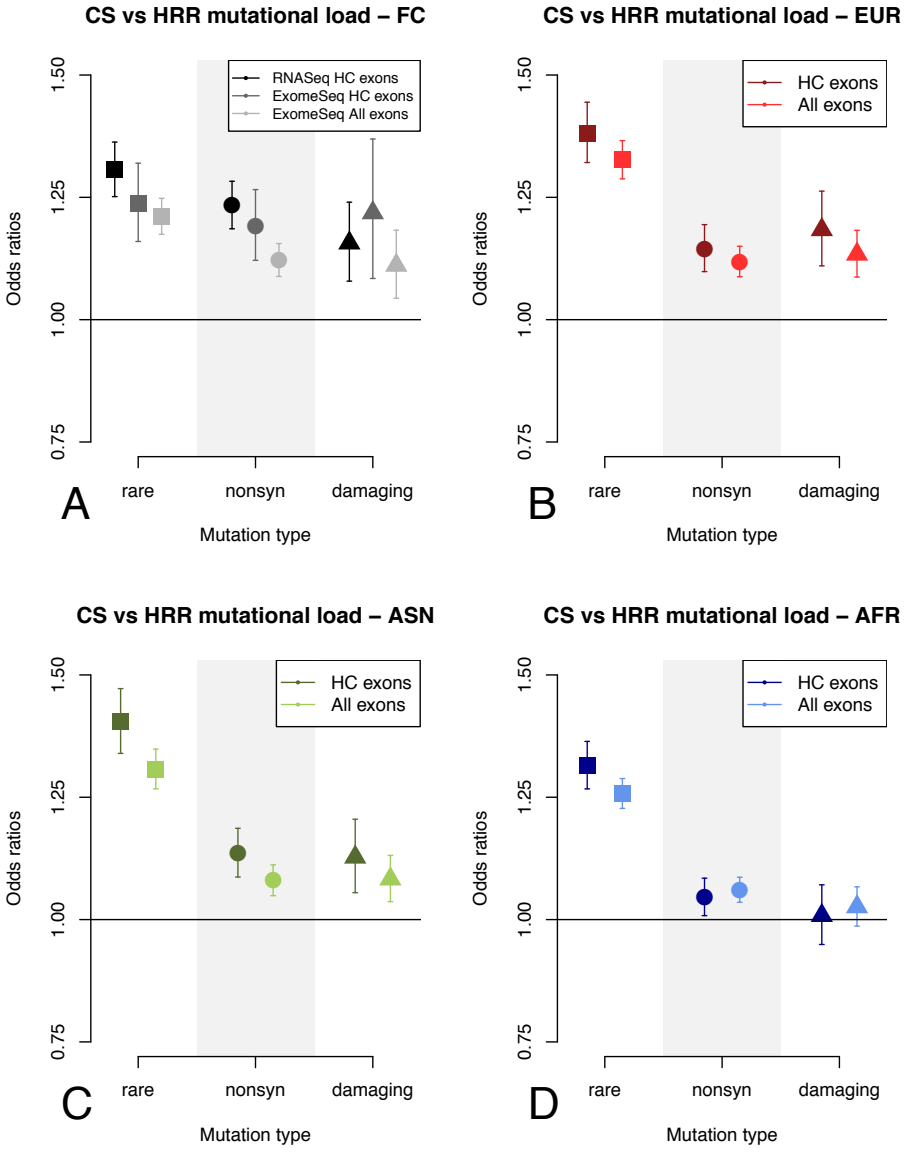

Figure S2. Differential mutational load in genomic subset of the data.

Differential load is computed using odds ratios (OR), representing the relative enrichment of a category of variants compared to all variants in CS vs. HRR for (A) RNA and exome sequencing of French-Canadians and for exome sequencing of (B) Europeans, (C) Asians and (D) Africans, from the 1000 Genome Project. Variants are categorized as rare (MAF<0.01 in a population), non-synonymous (missense and nonsense) and damaging (predicted by both SIFT and Polyphen2). Highly covered exons (HC exons) have coverage above 20X for each position within the exons in all datasets. The set of exons analysed does not affect the results and the exome dataset in French-Canadians replicates the results found in RNAseq.

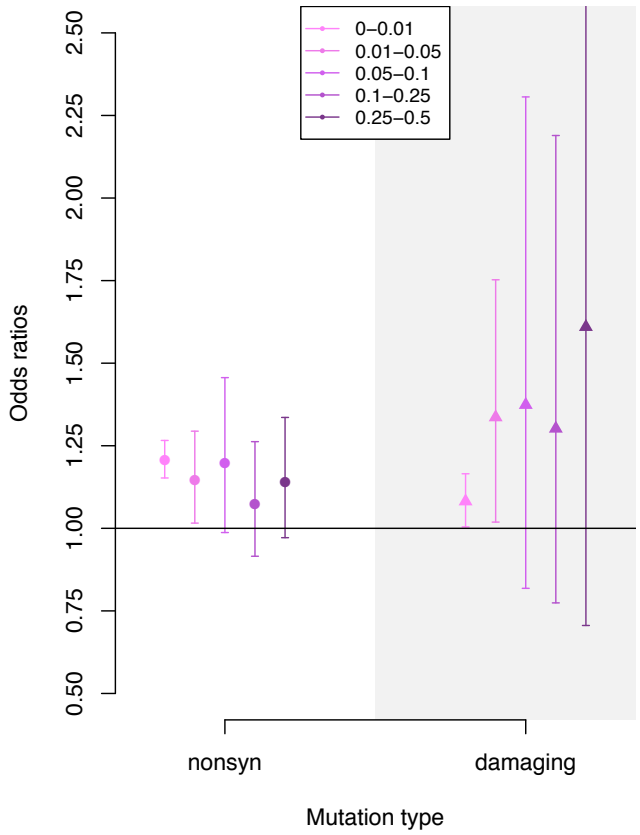

Figure S3. Effect of minor allele frequencies on odds ratios between CS and HRR (FCQ dataset)

Differential load is computed using odds ratios (OR) for mutations with different MAF in the FCQ dataset (RNAseq). The enrichment of non-synonymous and damaging mutations remains significant in the lower MAF classes (MAF<0.05), indicating that the excess of rare variants in CS does not drive the effect for non-synonymous and damaging variants.

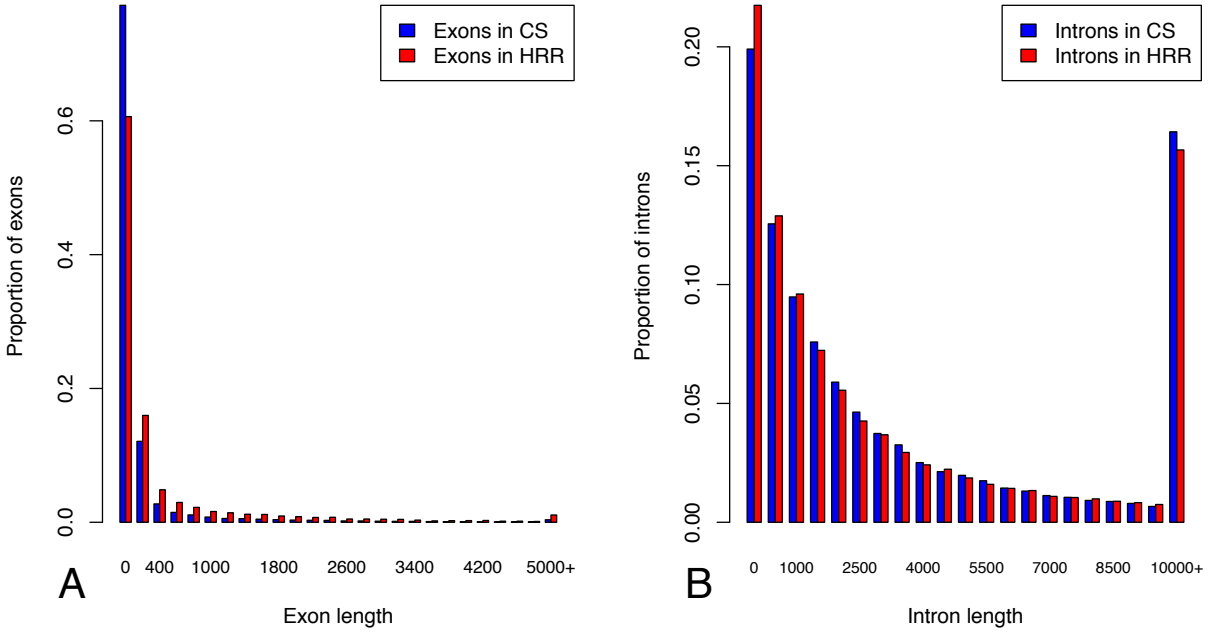

Figure S4. Distribution of exon and intron lengths in coldspots (CS) and high recombining regions (HRR).

(A) Exons are in bins of 250 bp. The last bin contains exons larger than 5 Kb. The mean length of exons in CS and HRR are 534 bp and 284 bp, respectively (B) Introns are in bins of 500 bp. The last bin contains exons larger than 10 Kb. The mean length of introns in CS and HRR are 7.075Kb and 7.026 Kb, respectively. Excluding introns longer than 10Kb, the mean length of introns in CS and HRR are 2.313 Kb and 2.260 Kb, respectively. The length distributions in CS and HRR are significantly different for exons (Kruskal-Wallis chi-squared = 2089.667, df = 1, p-value < 2. $\times 10^{-16}$) and for introns (Kruskal-Wallis chi-squared = 57.495, p = 3.388×10^{-14}).

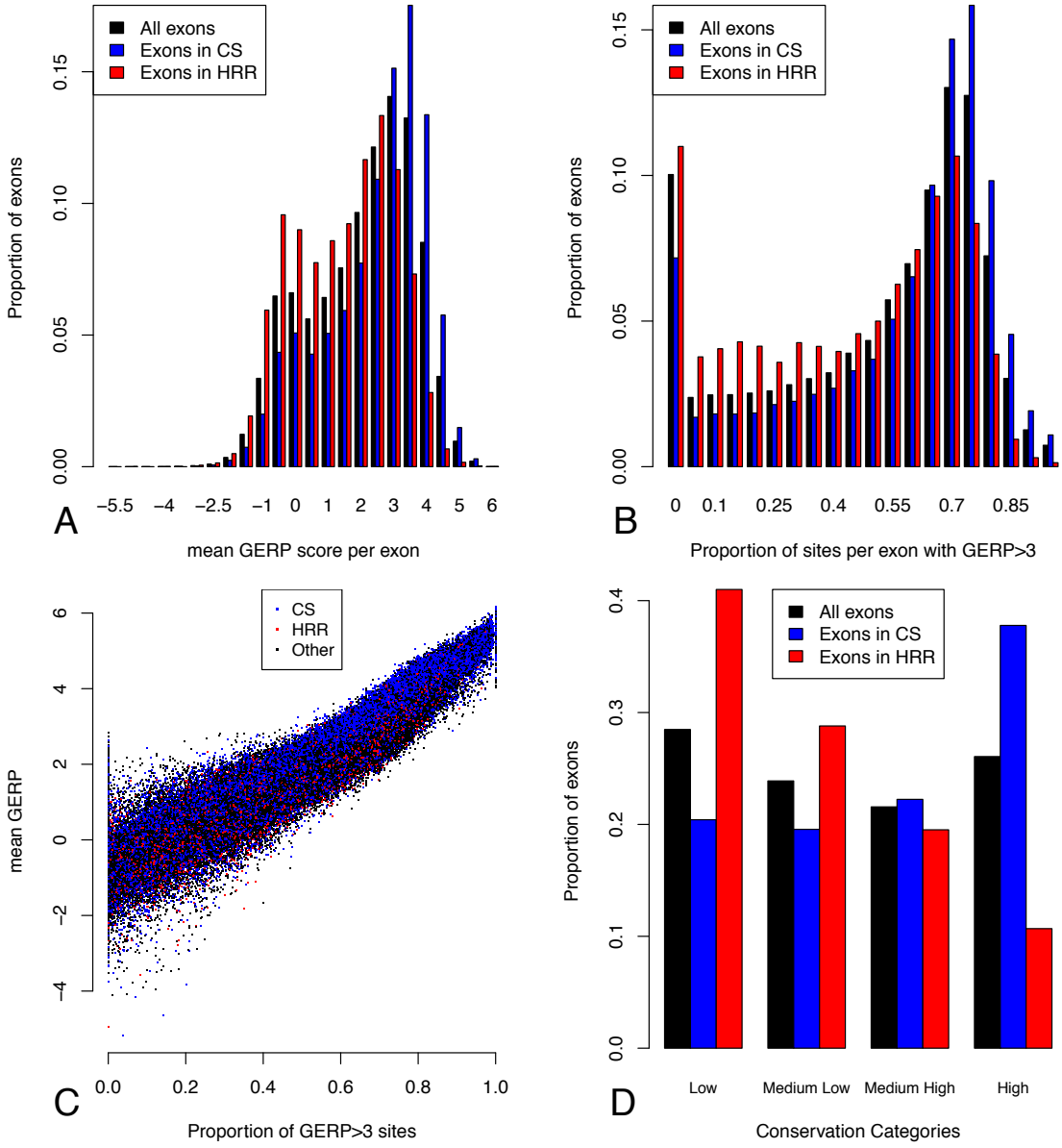

Figure S5. Distribution of conservation across exons measured by GERP scores.

(A) Mean GERP score per exon (B) Proportion of constrained positions (GERP>3) per exon (C) Scatter plot of mean GERP by the proportion of constrained positions for all exons (D) For each measure of conservation per exon, exons were grouped into 4 categories of equal sizes. Only exons that were concordant between the two classifications were kept in analyses within conservation categories, to minimize the effect of outliers with one of the two measures. Characteristics of exons in these four conservation categories in terms of average GERP score per base pair (bp) and number of constrained sites per bp (GERP>3) are reported in Figure 3C.

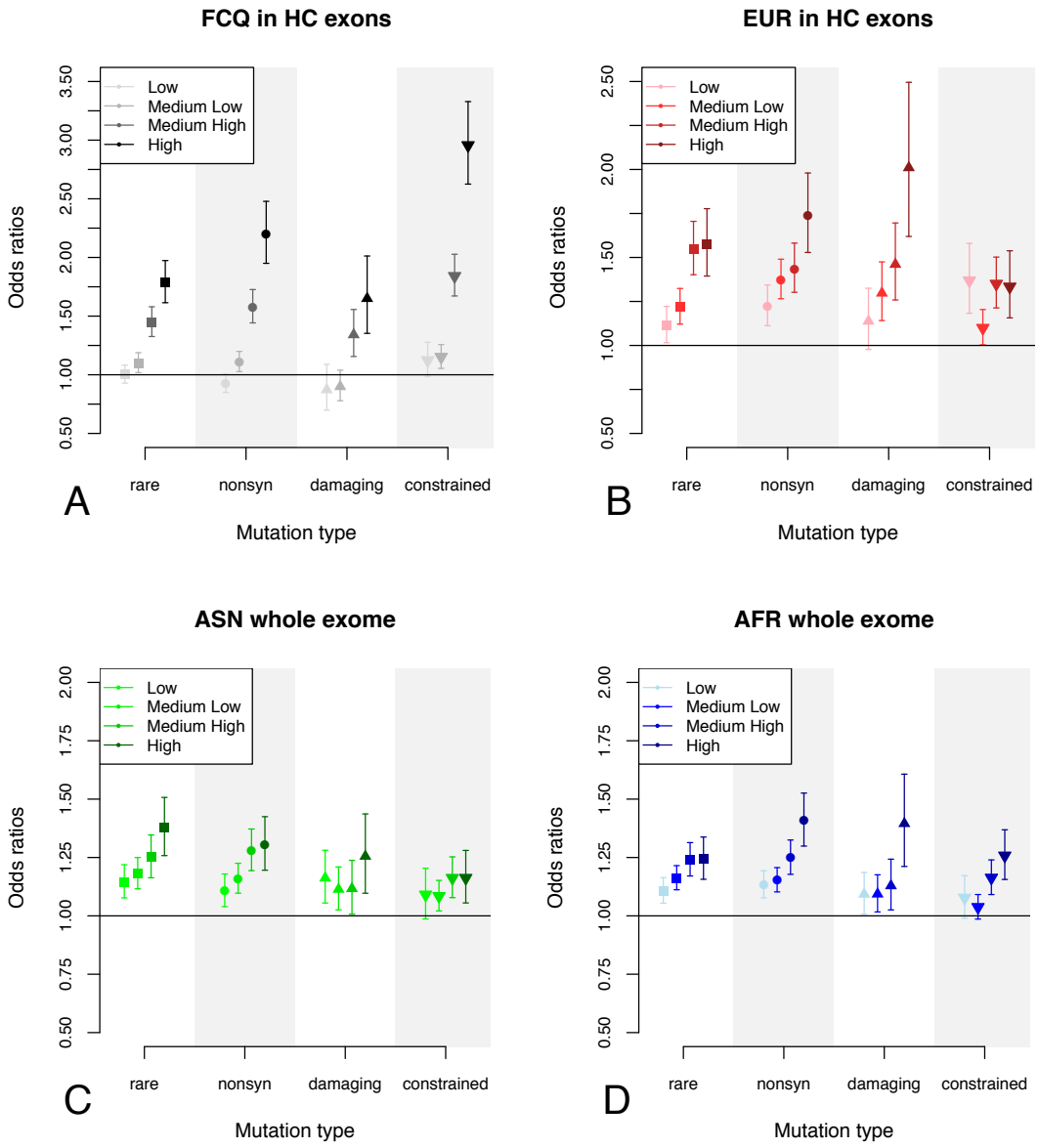

Figure S6. Differential Mutational Load in Conservation categories

Differential mutational load between coldspots (CS) and highly recombining regions (HRR) for rare (MAF<0.01), non-synonymous (nonsyn), damaging and constrained variants in (A) French-Canadians and (B) Europeans for Highly Covered (HC) exons, and in (C) Asians and (D) African for the whole exome. Results for Europeans in the whole exome are presented in Figure 3A. Results for Asians and Africans in HC exons (not shown), are similar to European results. For all populations and exon datasets, the Medium High and High conservation categories always show a significant enrichment for potentially deleterious mutations in CS.

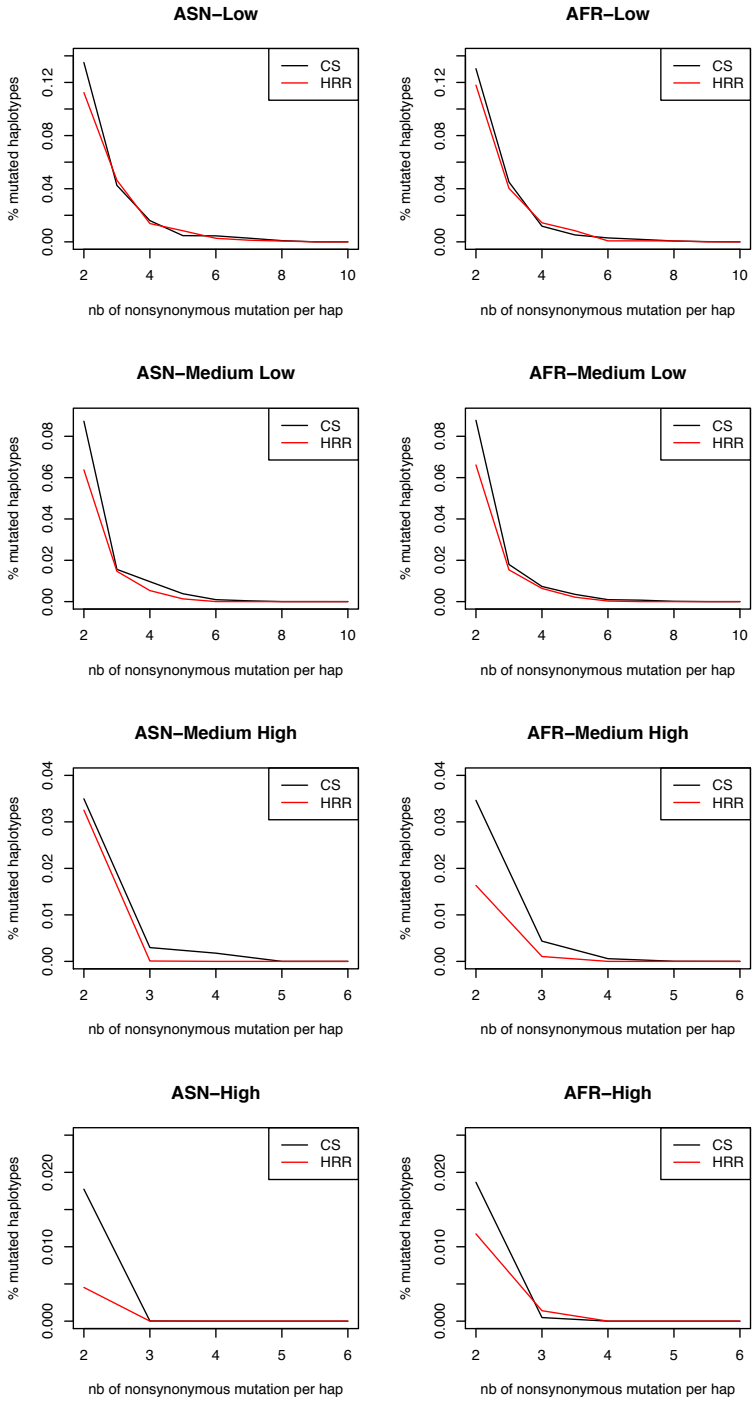

Figure S7. Haplotype load of non-synonymous variants in CS and HRR in Asians and Africans in the different conservation categories.

Haplotype load is computed as described in Material and Methods. Haplotype load in Europeans in presented in Figure 3B, with characteristics of conservation categories shown in Figure 3C.

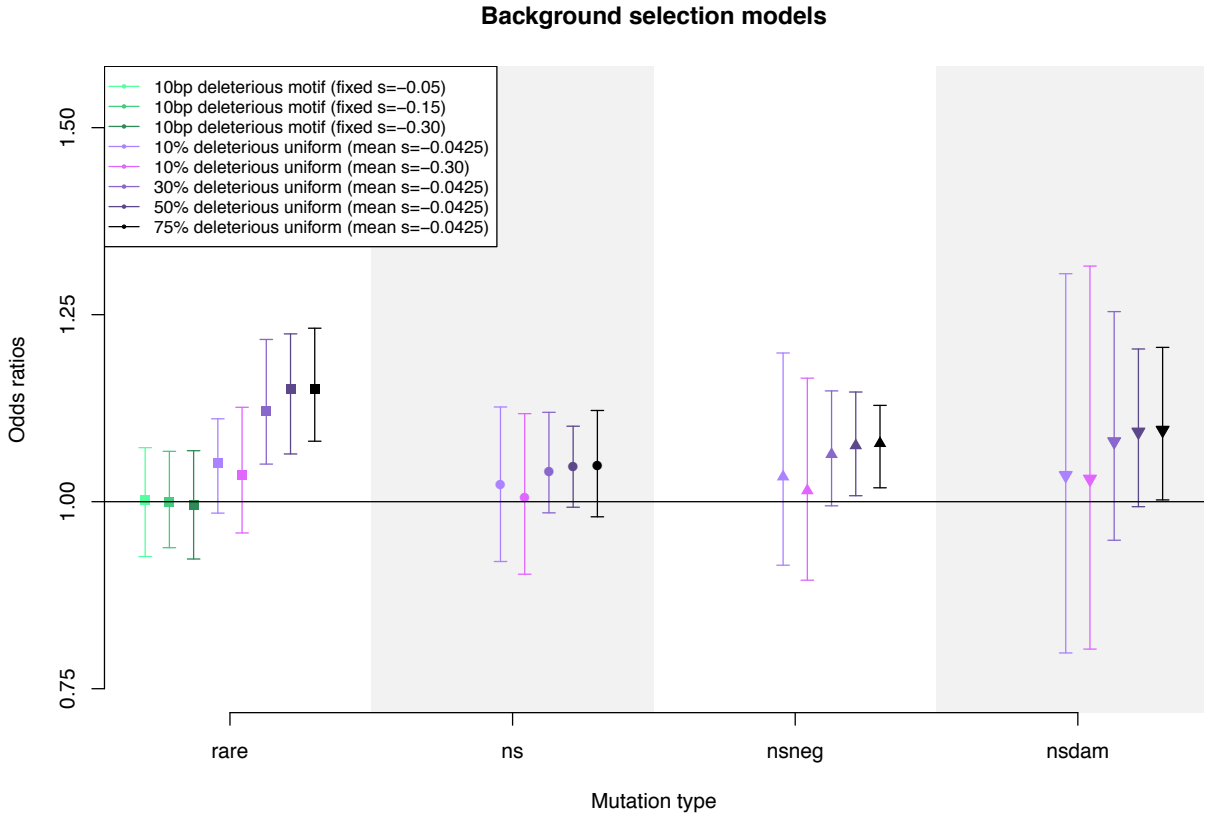

Figure S8. Simulations under different background selection models, with and without interference

Differential load is computed using odds ratios (OR), representing the relative enrichment of a category of variants (see description of *rare*, *ns*, *nsneg* and *nsdam* in online supplementary note 3) compared to all variants in simulated CS versus HRR. The models shown in green are background selection models without interference (only a small 10bp motif under negative selection is modelled with different fixed selection coefficients *s*). The other models have the same parameters as the EW model with θ=ρ (Table S6) and include selective interference with different proportion *p* of sites under negative selection. The model with *p*=75% of negatively selected sites (estimated proportion of non-synonymous sites in coding regions) recapitulates the empirical results the best.

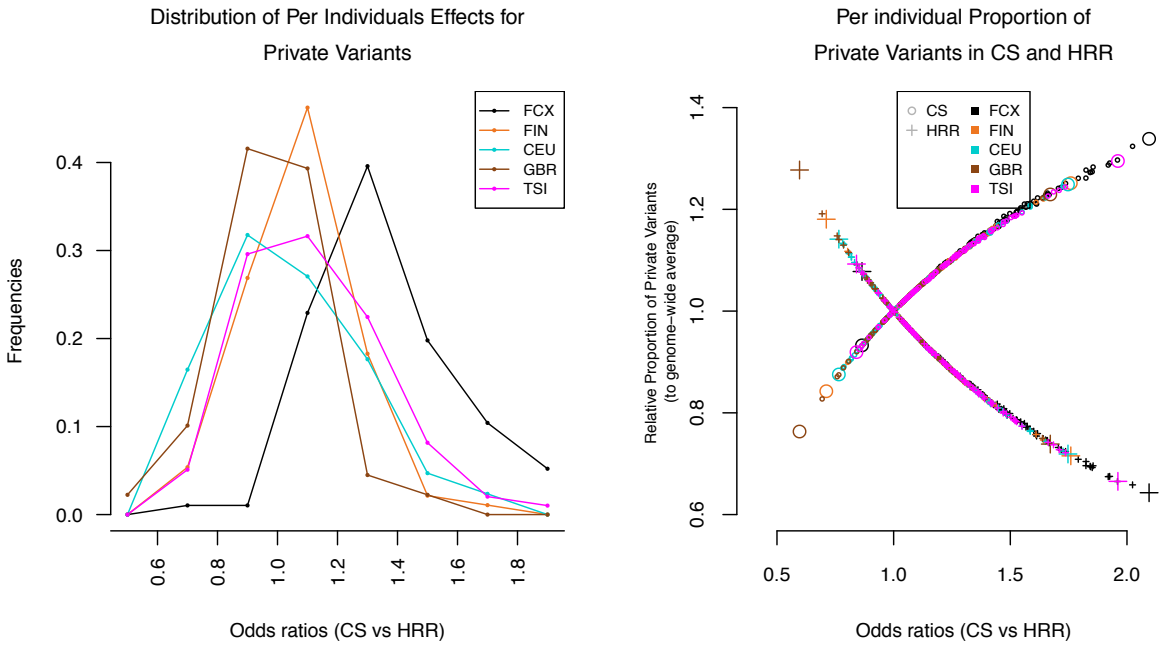

Figure S9. Per individual differential mutational load across European populations for private variants

Distribution of odds ratios (OR) per individual comparing proportions of private variants between CS and HRR in closely related populations of West European ancestry. OR are computed based on private variants called in the exome sequencing dataset of 96 French-Canadians (FCX), 89 British individuals (GBR), 93 Finns (FIN), 98 Italians from Tuscany (TSI) and 85 European Americans (CEU). The left panel shows the frequencies of individual OR in each population. The right panel shows, for each individual (ordered by their OR values), the relative proportions of private mutations in CS and HRR, computed by dividing CS and HRR proportions by genome-wide proportions of private variants within each individual, to adjust for differences across individuals.

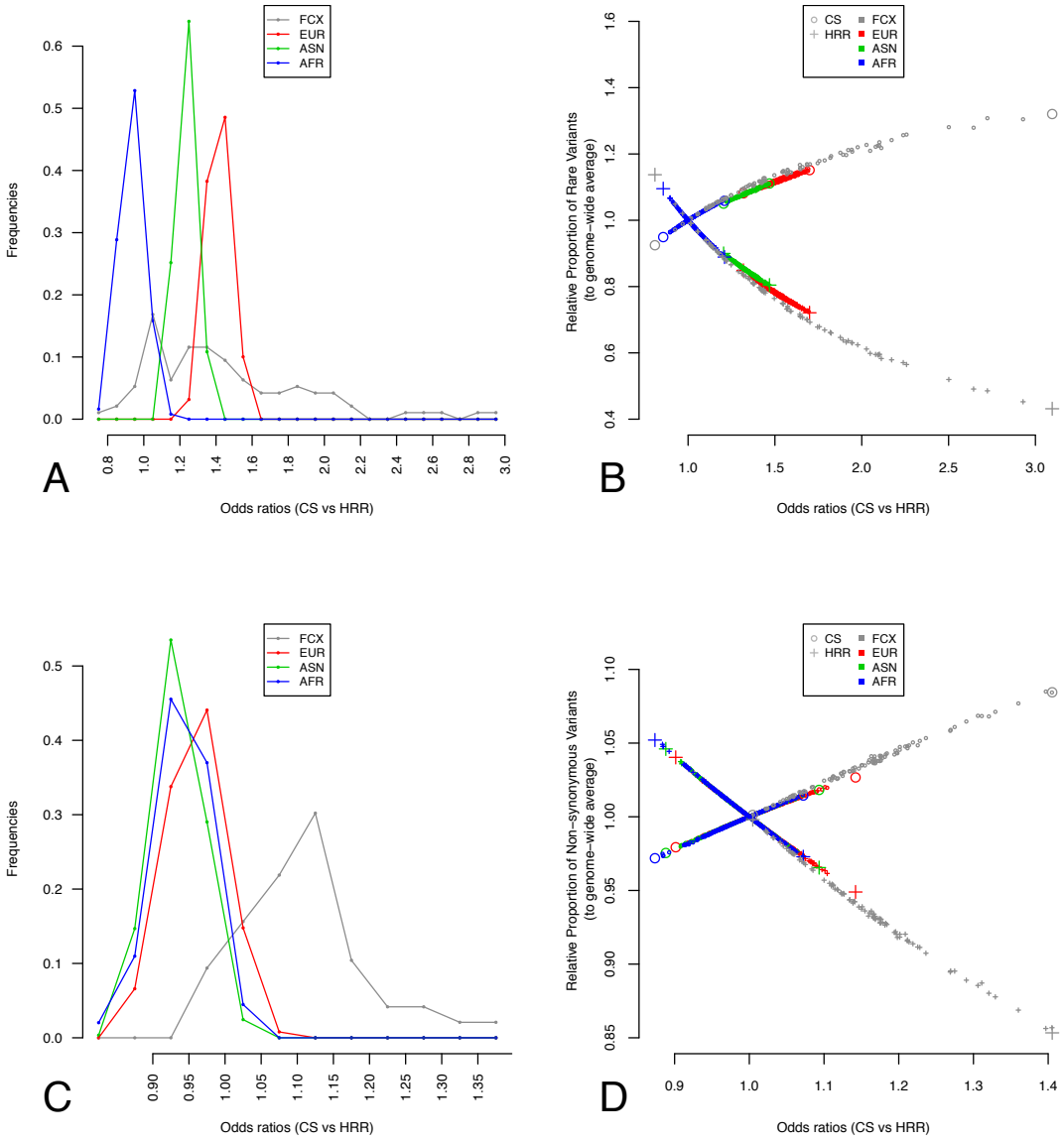

Figure S10. Per individual differential mutational load across populations with FCQ exome sequencing data.

Distribution of odds ratios (OR) per individual comparing proportions of rare (A, B) and non-synonymous (C, D) mutations between CS and HRR. For Europeans, Asians and Africans, the results are the same as shown in Figure 4, whereas French-Canadian results are computed using the exome sequencing dataset from 96 individuals. Further descriptions of the plots are found in Figure 4.

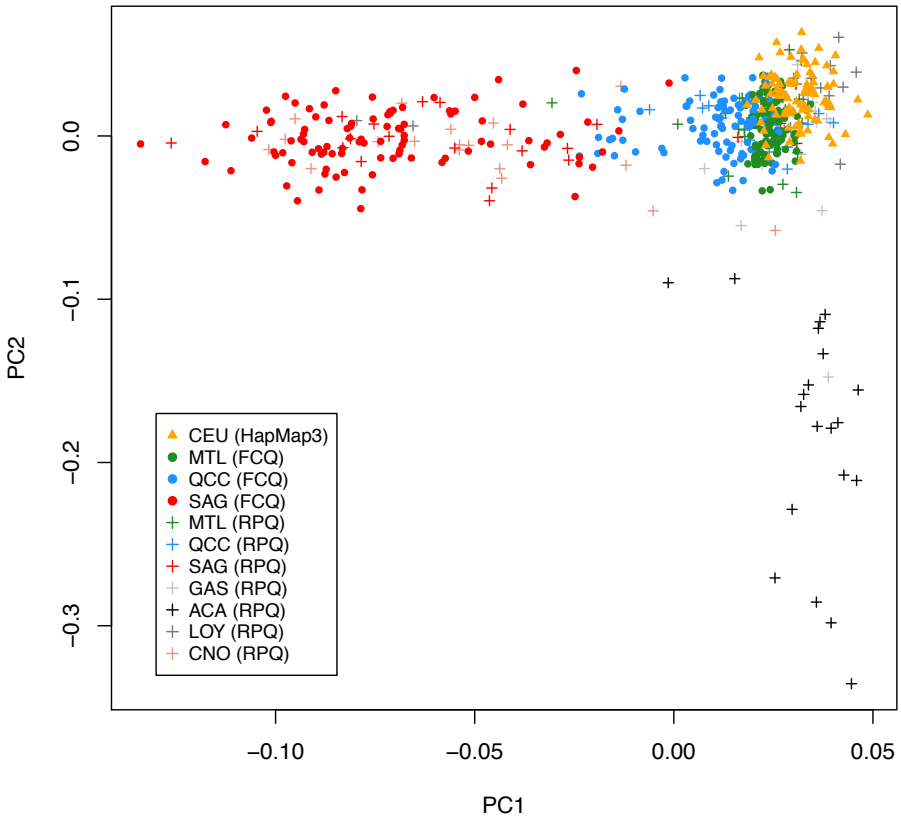

Figure S11. Population structure in regional populations of Quebec

Sampling from the CARTaGENE Project includes individuals from the Montreal area (MTL). Quebec City (QCC) and the Saguenay region (SAG). Regional origin of individuals was confirmed by a principal component analysis of genetic diversity in FCQ individuals compared with genetic diversity within the Reference Panel of Quebec (RPQ) and in the CEU population from HapMap3. Other populations included in the RPQ are : GAS : Gaspesia Region. ACA : Acadians. LOY : Loyalists. CNO : North Shore Region (*45*). [Canada map from http://atlas.gc.ca]

Supplementary Tables

Table S1. Distribution of sequence (A) and SNPs (B) in Coldspots (CS) and High Recombination Regions (HRR) genome-wide and in highly covered (HC) exons.

A

Regions	CS (bp)	HRR (bp)
Whole genome	1.048.937.114	634.243.758
Whole exome	25.302.008	17.768.017
HC exons	6.906.137	2.036.963

The reference genome hg19 contains 3.268.604.222 autosomal positions in total. The whole-exome includes 66.617.267 bp of sequences and the HC exons include 15.333.786 bp of sequences.

B

POP[a]	Number of individuals	Number of SNPs Whole Datasets			Number of SNPs HC exons[b]		
		TOTAL	HRR	CS	TOTAL	HRR	CS
FCQ	521	178.394	37.076	69.295	73.627	14.899	30.734
EUR	379	142.296	34.248	48.665	69.672	12.489	29.827
ASN	286	128.697	31.372	44.292	63.726	11.358	27.562
AFR	246	186.549	45.816	62.944	89.789	16.464	38.157

[a] French-Canadians (FCQ) Europeans (EUR). Asians (ASN) and Africans (AFR).

Table S2. Summary of linear regression models (FCQ dataset).

Variable	Rec rates[a]	GC content	Expression	Exon Size	SNPs/Kb	R^2
SNP/Kb	+ ***	+ ***	+ ***	NS	NA	0.038
Average MAF	+ ***	+ ***	+ ***	+ ***	NA	0.046
Expression[b]	- ***	+ ***	NA	NS	NA	0.016
Density (SNP/Kb) for						
Constrained	- ***	NS	NS	- ***	+ ***	0.267
Non-synonymous	-*	- **	- ***	- ***	+ ***	0.538
Damaging	NS	NS	- ***	- ***	+ ***	0.151
Private	- ***	+ ***	NS	NS	+ ***	0.387

*** p<0.001; ** p<0.01; * p<0.05; NS : non-significant; +/- = positive/negative correlation; NA : non-applicable.

[a] Average recombination rates per exon in cM/Mb are computed based on the FCQ genetic map.

[b] This correlation is evaluated considering all exons with minimum coverage of 20x in at 50% individuals. It is therefore biased against low expression genes.

Table S3. Robustness of the effect to GC-content. gene expression levels and divergence (FCQ dataset).

Odds ratio (OR) values comparing proportions of variants between coldspots and HRR are reported.

Feature	Category	OR Non-synonymous	OR Rare
GC-content (% GC per exon)	Low	1.543	1.407
	Medium Low	1.510	1.584
	Medium High	1.273	1.412
	High	NS	1.230
Average Expression (gene expression levels based on RNAseq FCQ dataset)	Low	1.226	1.317
	Medium Low	1.182	1.257
	Medium High	1.085	1.272
	High	1.328	1.435
Divergence to Chimpanzee (dS per exon computed by PAML)	Low	1.22	1.18
	Medium Low	1.18	1.25
	Medium High	1.28	1.42
	High	1.18	1.34
All categories		1.232	1.305

See Material and Methods for description of categories. NS: non-significant

Table S4. Effects for different mutation types (FCQ dataset).

Mutation type	OR Rare [CI 95%]	OR Non-synonymous [CI 95%]
GC→CG	1.44 [1.24;1.67]	1.49 [1.3;1.71]
GC→AT	1.5 [1.38;1.64]	1.11 [1.03;1.21]
AT→GC	1.39 [1.08;1.79]	1.29 [1.03;1.63]
AT→TA	1.25 [1.18;1.32]	1.25 [1.19;1.32]

Table S5. Robustness of the effect to the choice of recombination parameters (FCQ dataset)

Rec. rates (cM/Mb)		Odds ratios CS vs HRRs			Number of SNPs		
L	H	Non-synonymous	Rare	Private	CS	HRR	In between
	5	1.29	1.34	1.27	9263	15208	49159
0.1	10	1.25	1.33	1.26	9263	10406	53961
	20	1.2	1.26	1.17	9263	7517	56850
	5	1.24	1.32	1.25	20482	15054	38094
0.25	10	1.21	1.31	1.24	20482	10210	42938
	20	1.16	1.24	1.21	20482	7272	45876
	5	**1.23**	**1.31**	**1.25**	**30789**	**14902**	**27939**
0.5	10	1.21	1.31	1.25	30789	9903	32938
	20	1.17	1.25	1.17	30789	6857	35984
	5	1.19	1.27	1.22	41034	14770	17826
1	10	1.17	1.27	1.23	41034	9620	22976
	20	1.13	1.2	1.13	41034	6352	26244
	5	1.15	1.24	1.19	49583	14915	9132
2	10	1.15	1.25	1.21	49583	9389	14658
	20	1.12	1.19	1.12	49583	5892	18155

Coldspots Regions : SNPs within a 50Kb region with no recombination rate higher than L

High Recombination Regions (HRRs): SNPs within 50Kb of at least two hotspots with rate higher than H

Parameters used in this study are presented in red and were chosen to maximize the overall number of SNPs included in the analyses while minimizing the difference between the number of SNPs in coldspots and in HRRs

Table S6. Demographic and selection models used in simulations

Model	Parameters				
	θ	ρ	Genetic Map	Demography	Mean s[a]
EW θ=ρ	0.001	0.001	CS/HRR	constant size	-0.0425
EW θ=2ρ	0.001	0.0005	CS/HRR	constant size	-0.0425
AA θ=ρ	0.001	0.001	CS/HRR	expansion	-0.0294
AA θ=2ρ	0.001	0.0005	CS/HRR	expansion	-0.0294
EA θ=ρ	0.001	0.001	CS/HRR	bottleneck + expansion	-0.03
EA θ=2ρ	0.001	0.0005	CS/HRR	bottleneck + expansion	-0.03
EW constant ρ	0.001	0.001	constant rate	constant size	-0.0425
NTR	0.001	0.001	CS/HRR	constant size	0

[a] Negative selection is modelled by a gamma distribution of mean s. with p=75% of mutations attributed a non-zero selective coefficients

EW : DFE from Eyre-Walker et al. 2006

EA : DFE and demographic model from Boyko et al. 2008 for European-Americans

AA : DFE and demographic model from Boyko et al. 2008 for African-Americans

NTR : No selection

Table S7. Differential Mutational and Haplotype Load in CS versus HRR in Simulations

rare : derived allele frequency (DAF) <0.01; ns : non-synonymous with $s > -1/N_0$; nsneg : non-synonymous with $s < -1/N_0$; nsdam : non-synonymous with $s < 1\%$.

A

Mutation Type	Odds Ratios for Different Models							
	EW θ=ρ [CI 95%]		**EW θ=2ρ [CI 95%]**		**Constant ρ [CI 95%]**		**NTR [CI 95%]**	
rare	**1.22**	[1.12;1.29]	**1.14**	[1.08;1.2]	0.97	[0.9;1.05]	0.998	[0.92;1.07]
ns	1.05	[0.999;1.12]	1.04	[0.99;1.09]	0.99	[0.94;1.05]	-	-
nsneg	**1.1**	[1.04;1.16]	**1.06**	[1.01;1.12]	0.99	[0.93;1.06]	-	-
nsdam	**1.12**	[1.03;1.19]	**1.08**	[1.02;1.16]	0.98	[0.9;1.09]	-	-
	AA θ=ρ [CI 95%]		**AA θ=2ρ [CI 95%]**		**EA θ=ρ [CI 95%]**		**EA θ=2ρ [CI 95%]**	
rare	**1.18**	[1.14;1.23]	**1.14**	[1.09;1.19]	**1.21**	[1.14;1.27]	**1.14**	[1.09;1.22]
ns	1.03	[0.998;1.07]	1.02	[0.98;1.06]	1.03	[0.99;1.07]	1.02	[0.98;1.05]
nsneg	**1.06**	[1.02.1.1]	**1.04**	[1.002;1.09]	**1.05**	[1.01;1.09]	1.03	[0.99;1.08]
nsdam	**1.09**	[1.01;1.17]	1.07	[0.99;1.14]	1.06	[0.998;1.14]	1.04	[0.99;1.11]

Values in bold represent OR significantly different from 1.

B

Models	Mutation Type			
	rare	**ns**	**nsneg**	**nsdam**
EW θ=ρ, *p*=0.75	**<0.01**	0.13	**<0.01**	**0.01**
AA θ=ρ	**<0.01**	0.11	**0.01**	**<0.01**
EA θ=ρ	**<0.01**	0.05	**0.01**	**<0.01**
EW θ=ρ, *p*=0.1	**0.03**	0.42	0.35	0.28
EW θ=ρ, *p*=0.5	**<0.01**	0.09	**<0.01**	**0.01**
10bp deleterious motif (*s* = 0.1)	0.55	-	-	-
EW Constant ρ	0.74	0.54	0.68	0.69
NTR	0.56	-	-	-

Proportion of simulated replicate where haplotypes in HRR have a higher proportion of a given mutation type. Values in bold represent significant results (one-tailed p-value <0.05).

Table S8. Gene Ontology Analysis

Terms	Number of genes[a]	WebGestalt p-value	PANTHER p-value
Biological processes			
cell cycle	750	1.93×10^{-15}	2.18×10^{-11}
mitosis	420	1.93×10^{-7}	1.13×10^{-8}
protein metabolic processes	1578	8.32×10^{-12}	2.50×10^{-9}
mRNA processing	246	1.22×10^{-3}	7.95×10^{-8}
organelle organisation	1065	3.56×10^{-14}	term not included
microtubule-based processes	246	3.08×10^{-9}	term not included
Molecular function			
Binding	5154	8.64×10^{-8}	5.87×10^{-13}
nucleotide binding	1192	3.00×10^{-13}	1.96×10^{-14}
RNA binding	435	2.08×10^{-6}	1.24×10^{-7}
ATP binding	772	2.77×10^{-13}	term not included
Catalytic Activity	2472	5.06×10^{-11}	2.75×10^{-26}
ligase	279	1.54×10^{-9}	1.38×10^{-11}
transferase	840	5.18×10^{-5}	1.99×10^{-7}

[a]The number of genes is the maximum number reported between WebGestalt and PANTHER

Table S9. Overrepresentation of cancer variants and sensitive genomic regions in coldspots.

	COUNTS (bp)		OR for CS vs HRR
	CS	HRR	
Whole Exome	25,302,008	17,768,017	
Cosmic mutations	574,072	316,080	**1.275 [1.270;1.281]**
segregating	16,254	12,648	0.902 [0.881;0.923]
non-segregating (MAF < 0.001)	557,818	303,432	**1.290 [1.285;1.296]**
Motifs in Khurana et al. 2013			
Sensitive motifs	2,087,033	963,237	**1.522 [1.518; 1.525]**
Ultra-sensitive motifs	165,453	17,859	**6.506 [6.406; 6.607]**

Sensitive and ultra-sensitive motifs display an ~40- and ~400-fold enrichment of disease-causing mutations found in Human Gene Mutation Database (HGMD), respectively (*46*).

REFERENCES

1. A. G. Hinch, A. Tandon, N. Patterson, Y. Song, N. Rohland, C. D. Palmer, G. K. Chen, K. Wang, S. G. Buxbaum, E. L. Akylbekova, M. C. Aldrich, C. B. Ambrosone, C. Amos, E. V. Bandera, S. I. Berndt, L. Bernstein, W. J. Blot, C. H. Bock, E. Boerwinkle, Q. Cai, N. Caporaso, G. Casey, L. A. Cupples, S. L. Deming, W. R. Diver, J. Divers, M. Fornage, E. M. Gillanders, J. Glessner, C. C. Harris, J. J. Hu, S. A. Ingles, W. Isaacs, E. M. John, W. H. Kao, B. Keating, R. A. Kittles, L. N. Kolonel, E. Larkin, L. Le Marchand, L. H. McNeill, R. C. Millikan, A. Murphy, S. Musani, C. Neslund-Dudas, S. Nyante, G. J. Papanicolaou, M. F. Press, B. M. Psaty, A. P. Reiner, S. S. Rich, J. L. Rodriguez-Gil, J. I. Rotter, B. A. Rybicki, A. G. Schwartz, L. B. Signorello, M. Spitz, S. S. Strom, M. J. Thun, M. A. Tucker, Z. Wang, J. K. Wiencke, J. S. Witte, M. Wrensch, X. Wu, Y. Yamamura, K. A. Zanetti, W. Zheng, R. G. Ziegler, X. Zhu, S. Redline, J. N. Hirschhorn, B. E. Henderson, H. A. Taylor, Jr., A. L. Price, H. Hakonarson, S. J. Chanock, C. A. Haiman, J. G. Wilson, D. Reich, S. R. Myers, The landscape of recombination in African Americans. *Nature* **476**, 170-175 (2011); published online EpubAug 11 (nature10336 [pii] 10.1038/nature10336).

2. A. Kong, G. Thorleifsson, D. F. Gudbjartsson, G. Masson, A. Sigurdsson, A. Jonasdottir, G. B. Walters, A. Gylfason, K. T. Kristinsson, S. A. Gudjonsson, M. L. Frigge, A. Helgason, U. Thorsteinsdottir, K. Stefansson, Fine-scale recombination rate differences between sexes, populations and individuals. *Nature* **467**, 1099-1103 (2010); published online EpubOct 28 (nature09525 [pii] 10.1038/nature09525).

3. HapMap Consortium, K. A. Frazer, D. G. Ballinger, D. R. Cox, D. A. Hinds, L. L. Stuve, R. A. Gibbs, J. W. Belmont, A. Boudreau, P. Hardenbol, S. M. Leal, S. Pasternak, D. A. Wheeler, T. D. Willis, F. Yu, H. Yang, C. Zeng, Y. Gao, H. Hu, W. Hu, C. Li, W. Lin, S. Liu, H. Pan, X. Tang, J. Wang, W. Wang, J. Yu, B. Zhang, Q. Zhang, H. Zhao, J. Zhou, S. B. Gabriel, R. Barry, B. Blumenstiel, A. Camargo, M. Defelice, M. Faggart, M. Goyette, S. Gupta, J. Moore, H. Nguyen, R. C. Onofrio, M. Parkin, J. Roy, E. Stahl, E. Winchester, L. Ziaugra, D. Altshuler, Y. Shen, Z. Yao, W. Huang, X. Chu, Y. He, L. Jin, Y. Liu, W. Sun, H. Wang, Y. Wang, X. Xiong, L. Xu, M. M. Waye, S. K. Tsui, H. Xue, J. T. Wong, L. M. Galver, J. B. Fan, K. Gunderson, S. S. Murray, A. R. Oliphant, M. S. Chee, A. Montpetit, F. Chagnon, V. Ferretti, M. Leboeuf, J. F. Olivier, M. S. Phillips, S. Roumy, C. Sallee, A. Verner, T. J. Hudson, P. Y. Kwok, D. Cai, D. C. Koboldt, R. D. Miller, L. Pawlikowska, P. Taillon-Miller, M. Xiao, L. C. Tsui, W. Mak, Y. Q. Song, P. K. Tam, Y. Nakamura, T. Kawaguchi, T. Kitamoto, T. Morizono, A. Nagashima, Y. Ohnishi, A. Sekine, T. Tanaka, T. Tsunoda, P. Deloukas, C. P. Bird, M. Delgado, E. T. Dermitzakis, R. Gwilliam, S. Hunt, J. Morrison, D. Powell, B. E. Stranger, P. Whittaker, D. R. Bentley, M. J. Daly, P. I. de Bakker, J. Barrett, Y. R. Chretien, J. Maller, S. McCarroll, N. Patterson, I. Pe'er, A. Price, S. Purcell, D. J. Richter, P. Sabeti, R. Saxena, S. F. Schaffner, P. C. Sham, P. Varilly, L. D. Stein, L. Krishnan, A. V. Smith, M. K. Tello-Ruiz, G. A. Thorisson, A. Chakravarti, P. E. Chen, D. J. Cutler, C. S. Kashuk, S. Lin, G. R. Abecasis, W. Guan, Y. Li, H. M. Munro, Z. S. Qin, D. J. Thomas, G. McVean, A. Auton, L. Bottolo, N. Cardin, S. Eyheramendy, C. Freeman, J. Marchini, S. Myers, C. Spencer, M.

Stephens, P. Donnelly, L. R. Cardon, G. Clarke, D. M. Evans, A. P. Morris, B. S. Weir, J. C. Mullikin, S. T. Sherry, M. Feolo, A. Skol, H. Zhang, I. Matsuda, Y. Fukushima, D. R. Macer, E. Suda, C. N. Rotimi, C. A. Adebamowo, I. Ajayi, T. Aniagwu, P. A. Marshall, C. Nkwodimmah, C. D. Royal, M. F. Leppert, M. Dixon, A. Peiffer, R. Qiu, A. Kent, K. Kato, N. Niikawa, I. F. Adewole, B. M. Knoppers, M. W. Foster, E. W. Clayton, J. Watkin, D. Muzny, L. Nazareth, E. Sodergren, G. M. Weinstock, I. Yakub, B. W. Birren, R. K. Wilson, L. L. Fulton, J. Rogers, J. Burton, N. P. Carter, C. M. Clee, M. Griffiths, M. C. Jones, K. McLay, R. W. Plumb, M. T. Ross, S. K. Sims, D. L. Willey, Z. Chen, H. Han, L. Kang, M. Godbout, J. C. Wallenburg, P. L'Archeveque, G. Bellemare, K. Saeki, D. An, H. Fu, Q. Li, Z. Wang, R. Wang, A. L. Holden, L. D. Brooks, J. E. McEwen, M. S. Guyer, V. O. Wang, J. L. Peterson, M. Shi, J. Spiegel, L. M. Sung, L. F. Zacharia, F. S. Collins, K. Kennedy, R. Jamieson, J. Stewart, A second generation human haplotype map of over 3.1 million SNPs. *Nature* **449**, 851-861 (2007); published online EpubOct 18 (nature06258 [pii]
10.1038/nature06258).

4. G. McVean, P. Awadalla, P. Fearnhead, A coalescent-based method for detecting and estimating recombination from gene sequences. *Genetics* **160**, 1231-1241 (2002); published online EpubMar (

5. O. Delaneau, J. F. Zagury, J. Marchini, Improved whole-chromosome phasing for disease and population genetic studies. *Nat Methods* **10**, 5-6 (2013); published online EpubJan (10.1038/nmeth.2307).

6. A. Kong, D. F. Gudbjartsson, J. Sainz, G. M. Jonsdottir, S. A. Gudjonsson, B. Richardsson, S. Sigurdardottir, J. Barnard, B. Hallbeck, G. Masson, A. Shlien, S. T. Palsson, M. L. Frigge, T. E. Thorgeirsson, J. R. Gulcher, K. Stefansson, A high-resolution recombination map of the human genome. *Nat Genet* **31**, 241-247 (2002); published online EpubJul (10.1038/ng917
ng917 [pii]).

7. P. Awadalla, C. Boileau, Y. Payette, Y. Idaghdour, J. P. Goulet, B. Knoppers, P. Hamet, C. Laberge, Cohort profile of the CARTaGENE study: Quebec's population-based biobank for public health and personalized genomics. *Int J Epidemiol*, (2012); published online EpubOct 15 (dys160 [pii]
10.1093/ije/dys160).

8. J. Hussin, M. H. Roy-Gagnon, R. Gendron, G. Andelfinger, P. Awadalla, Age-dependent recombination rates in human pedigrees. *PLoS Genet* **7**, e1002251 (2011); published online EpubSep (10.1371/journal.pgen.1002251
PGENETICS-D-11-00151 [pii]).

9. C. Bherer, D. Labuda, M. H. Roy-Gagnon, L. Houde, M. Tremblay, H. Vezina, Admixed ancestry and stratification of Quebec regional populations. *Am J Phys Anthropol* **144**, 432-441 (2011); published online EpubMar (10.1002/ajpa.21424).

10. C. Trapnell, L. Pachter, S. L. Salzberg, TopHat: discovering splice junctions with RNA-Seq. *Bioinformatics* **25**, 1105-1111 (2009); published online EpubMay 1 (btp120 [pii]
10.1093/bioinformatics/btp120).

11. F. E. Dewey, R. Chen, S. P. Cordero, K. E. Ormond, C. Caleshu, K. J. Karczewski, M. Whirl-Carrillo, M. T. Wheeler, J. T. Dudley, J. K. Byrnes, O. E. Cornejo, J. W. Knowles, M. Woon, K. Sangkuhl, L. Gong, C. F. Thorn, J. M. Hebert, E. Capriotti, S. P. David, A. Pavlovic, A. West, J. V. Thakuria, M. P. Ball, A. W. Zaranek, H. L. Rehm, G. M. Church, J. S. West, C. D. Bustamante, M. Snyder, R. B. Altman, T. E. Klein, A. J. Butte, E. A.

Ashley, Phased whole-genome genetic risk in a family quartet using a major allele reference sequence. *PLoS Genet* **7**, e1002280 (2011); published online EpubSep (10.1371/journal.pgen.1002280
PGENETICS-D-11-00831 [pii]).

12. S. Anders, W. Huber, Differential expression analysis for sequence count data. *Genome Biol* **11**, R106 (2010)gb-2010-11-10-r106 [pii]
10.1186/gb-2010-11-10-r106).
13. J. H. Bullard, E. Purdom, K. D. Hansen, S. Dudoit, Evaluation of statistical methods for normalization and differential expression in mRNA-Seq experiments. *BMC Bioinformatics* **11**, 94 (2010)1471-2105-11-94 [pii]
10.1186/1471-2105-11-94).
14. D. Risso, K. Schwartz, G. Sherlock, S. Dudoit, GC-content normalization for RNA-Seq data. *BMC Bioinformatics* **12**, 480 (2011)1471-2105-12-480 [pii]
10.1186/1471-2105-12-480).
15. B. Langmead, C. Trapnell, M. Pop, S. L. Salzberg, Ultrafast and memory-efficient alignment of short DNA sequences to the human genome. *Genome Biol* **10**, R25 (2009)gb-2009-10-3-r25 [pii]
10.1186/gb-2009-10-3-r25).
16. A. McKenna, M. Hanna, E. Banks, A. Sivachenko, K. Cibulskis, A. Kernytsky, K. Garimella, D. Altshuler, S. Gabriel, M. Daly, M. A. DePristo, The Genome Analysis Toolkit: a MapReduce framework for analyzing next-generation DNA sequencing data. *Genome Res* **20**, 1297-1303 (2010); published online EpubSep (gr.107524.110 [pii]
10.1101/gr.107524.110).
17. H. Li, B. Handsaker, A. Wysoker, T. Fennell, J. Ruan, N. Homer, G. Marth, G. Abecasis, R. Durbin, The Sequence Alignment/Map format and SAMtools. *Bioinformatics* **25**, 2078-2079 (2009); published online EpubAug 15 (btp352 [pii]
10.1093/bioinformatics/btp352).
18. P. Danecek, A. Auton, G. Abecasis, C. A. Albers, E. Banks, M. A. DePristo, R. E. Handsaker, G. Lunter, G. T. Marth, S. T. Sherry, G. McVean, R. Durbin, The variant call format and VCFtools. *Bioinformatics* **27**, 2156-2158 (2011); published online EpubAug 1 (btr330 [pii]
10.1093/bioinformatics/btr330).
19. I. Gordo, B. Charlesworth, The speed of Muller's ratchet with background selection, and the degeneration of Y chromosomes. *Genet Res* **78**, 149-161 (2001); published online EpubOct (
20. G. A. McVean, B. Charlesworth, The effects of Hill-Robertson interference between weakly selected mutations on patterns of molecular evolution and variation. *Genetics* **155**, 929-944 (2000); published online EpubJun (
21. J. Felsenstein, The evolutionary advantage of recombination. *Genetics* **78**, 737-756 (1974); published online EpubOct (
22. R. J. Soderberg, O. G. Berg, Mutational interference and the progression of Muller's ratchet when mutations have a broad range of deleterious effects. *Genetics* **177**, 971-986 (2007); published online EpubOct (10.1534/genetics.107.073791).
23. P. D. Keightley, S. P. Otto, Interference among deleterious mutations favours sex and recombination in finite populations. *Nature* **443**, 89-92 (2006); published online EpubSep 7 (10.1038/nature05049).

24. B. Charlesworth, D. Charlesworth, Rapid fixation of deleterious alleles can be caused by Muller's ratchet. *Genet Res* **70**, 63-73 (1997); published online EpubAug (
25. P. W. Messer, SLiM: simulating evolution with selection and linkage. *Genetics* **194**, 1037-1039 (2013); published online EpubAug (10.1534/genetics.113.152181).
26. R. D. Hernandez, A flexible forward simulator for populations subject to selection and demography. *Bioinformatics* **24**, 2786-2787 (2008); published online EpubDec 1 (10.1093/bioinformatics/btn522).
27. A. Eyre-Walker, M. Woolfit, T. Phelps, The distribution of fitness effects of new deleterious amino acid mutations in humans. *Genetics* **173**, 891-900 (2006); published online EpubJun (genetics.106.057570 [pii]
10.1534/genetics.106.057570).
28. A. R. Boyko, S. H. Williamson, A. R. Indap, J. D. Degenhardt, R. D. Hernandez, K. E. Lohmueller, M. D. Adams, S. Schmidt, J. J. Sninsky, S. R. Sunyaev, T. J. White, R. Nielsen, A. G. Clark, C. D. Bustamante, Assessing the evolutionary impact of amino acid mutations in the human genome. *PLoS Genet* **4**, e1000083 (2008); published online EpubMay (10.1371/journal.pgen.1000083).
29. N. Ray, M. Currat, M. Foll, L. Excoffier, SPLATCHE2: a spatially explicit simulation framework for complex demography, genetic admixture and recombination. *Bioinformatics* **26**, 2993-2994 (2010); published online EpubDec 1 (10.1093/bioinformatics/btq579).
30. F. Austerlitz, E. Heyer, Social transmission of reproductive behavior increases frequency of inherited disorders in a young-expanding population. *Proc Natl Acad Sci U S A* **95**, 15140-15144 (1998); published online EpubDec 8 (
31. C. Moreau, C. Bherer, H. Vezina, M. Jomphe, D. Labuda, L. Excoffier, Deep human genealogies reveal a selective advantage to be on an expanding wave front. *Science* **334**, 1148-1150 (2011); published online EpubNov 25 (10.1126/science.1212880).
32. S. M. Hoban, M. Mezzavilla, O. E. Gaggiotti, A. Benazzo, C. van Oosterhout, G. Bertorelle, High variance in reproductive success generates a false signature of a genetic bottleneck in populations of constant size: a simulation study. *BMC Bioinformatics* **14**, 309 (2013); published online EpubOct 16 (10.1186/1471-2105-14-309).
33. Y. B. Simons, M. C. Turchin, J. K. Pritchard, G. Sella, The deleterious mutation load is insensitive to recent population history. *Nat Genet*, (2014); published online EpubFeb 9 (10.1038/ng.2896).
34. I. A. Adzhubei, S. Schmidt, L. Peshkin, V. E. Ramensky, A. Gerasimova, P. Bork, A. S. Kondrashov, S. R. Sunyaev, A method and server for predicting damaging missense mutations. *Nat Methods* **7**, 248-249 (2010); published online EpubApr (nmeth0410-248 [pii]
10.1038/nmeth0410-248).
35. P. Kumar, S. Henikoff, P. C. Ng, Predicting the effects of coding non-synonymous variants on protein function using the SIFT algorithm. *Nat Protoc* **4**, 1073-1081 (2009)nprot.2009.86 [pii]
10.1038/nprot.2009.86).
36. S. E. Flanagan, A. M. Patch, S. Ellard, Using SIFT and PolyPhen to predict loss-of-function and gain-of-function mutations. *Genet Test Mol Biomarkers* **14**, 533-537 (2010); published online EpubAug (10.1089/gtmb.2010.0036).
37. C. Pal, B. Papp, M. J. Lercher, An integrated view of protein evolution. *Nat Rev Genet* **7**, 337-348 (2006); published online EpubMay (nrg1838 [pii]

10.1038/nrg1838).

38. A. Necsulea, M. Semon, L. Duret, L. D. Hurst, Monoallelic expression and tissue specificity are associated with high crossover rates. *Trends Genet* **25**, 519-522 (2009); published online EpubDec (S0168-9525(09)00187-5 [pii]
10.1016/j.tig.2009.10.001).
39. J. M. Comeron, M. Kreitman, The correlation between intron length and recombination in drosophila. Dynamic equilibrium between mutational and selective forces. *Genetics* **156**, 1175-1190 (2000); published online EpubNov (
40. A. B. Carvalho, A. G. Clark, Intron size and natural selection. *Nature* **401**, 344 (1999); published online EpubSep 23 (10.1038/43827).
41. D. Wang, J. Yu, Both size and GC-content of minimal introns are selected in human populations. *PLoS One* **6**, e17945 (2011)10.1371/journal.pone.0017945).
42. J. L. Campos, B. Charlesworth, P. R. Haddrill, Molecular evolution in nonrecombining regions of the Drosophila melanogaster genome. *Genome Biol Evol* **4**, 278-288 (2012)10.1093/gbe/evs010).
43. X. Hong, D. G. Scofield, M. Lynch, Intron size, abundance, and distribution within untranslated regions of genes. *Mol Biol Evol* **23**, 2392-2404 (2006); published online EpubDec (10.1093/molbev/msl111).
44. M. Ashburner, C. A. Ball, J. A. Blake, D. Botstein, H. Butler, J. M. Cherry, A. P. Davis, K. Dolinski, S. S. Dwight, J. T. Eppig, M. A. Harris, D. P. Hill, L. Issel-Tarver, A. Kasarskis, S. Lewis, J. C. Matese, J. E. Richardson, M. Ringwald, G. M. Rubin, G. Sherlock, Gene ontology: tool for the unification of biology. The Gene Ontology Consortium. *Nat Genet* **25**, 25-29 (2000); published online EpubMay (10.1038/75556).
45. M. H. Roy-Gagnon, C. Moreau, C. Bherer, P. St-Onge, D. Sinnett, C. Laprise, H. Vezina, D. Labuda, Genomic and genealogical investigation of the French Canadian founder population structure. *Hum Genet* **129**, 521-531 (2011); published online EpubMay (10.1007/s00439-010-0945-x).
46. E. Khurana, Y. Fu, V. Colonna, X. J. Mu, H. M. Kang, T. Lappalainen, A. Sboner, L. Lochovsky, J. Chen, A. Harmanci, J. Das, A. Abyzov, S. Balasubramanian, K. Beal, D. Chakravarty, D. Challis, Y. Chen, D. Clarke, L. Clarke, F. Cunningham, U. S. Evani, P. Flicek, R. Fragoza, E. Garrison, R. Gibbs, Z. H. Gumus, J. Herrero, N. Kitabayashi, Y. Kong, K. Lage, V. Liluashvili, S. M. Lipkin, D. G. MacArthur, G. Marth, D. Muzny, T. H. Pers, G. R. Ritchie, J. A. Rosenfeld, C. Sisu, X. Wei, M. Wilson, Y. Xue, F. Yu, C. Genomes Project, E. T. Dermitzakis, H. Yu, M. A. Rubin, C. Tyler-Smith, M. Gerstein, Integrative annotation of variants from 1092 humans: application to cancer genomics. *Science* **342**, 1235587 (2013); published online EpubOct 4 (10.1126/science.1235587).